
Article:
Jeffries, R.D., Oliveira, J.M., Naylor, T. et al. (2 more authors) (2007) The Keele-Exeter young cluster survey - I. Low-mass pre-main-sequence stars in NGC 2169. Monthly Notices of the Royal Astronomical Society, 376 (2). pp. 580-598. ISSN 0035-8711

https://doi.org/10.1111/j.1365-2966.2007.11327.x

Mon. Not. R. Astron. Soc. **376,** 580–598 (2007) doi:10.1111/j.1365-2966.2007.11327.x

The Keele–Exeter young cluster survey – I. Low-mass pre-main-sequence stars in NGC 2169

R. D. Jeffries,[1⋆] J. M. Oliveira,[1] Tim Naylor,[2] N. J. Mayne[2] and S. P. Littlefair[2,3]

[1]*Astrophysics Group, School of Physical and Geographical Sciences, Keele University, Keele, Staffordshire ST5 5BG*
[2]*School of Physics, University of Exeter, Stocker Road, Exeter EX4 4QL*
[3]*Department of Physics and Astronomy, University of Sheffield, Sheffield S3 7RH*

Accepted 2006 November 21. Received 2006 November 20; in original form 2006 September 5

ABSTRACT

We have used $R_C I_C$ CCD photometry from the Isaac Newton telescope and intermediate-resolution spectroscopy from the *Gemini* North telescope to identify and characterize low-mass ($0.15 < M/\mathrm{M}_\odot < 1.3$) pre-main-sequence stars in the young open cluster NGC 2169. Isochrone fitting to the high- and low-mass populations yields an intrinsic distance modulus of $10.13^{+0.06}_{-0.09}$ mag and a model-dependent age of 9 ± 2 Myr. Compared to the nearby, kinematically defined groups of a similar age, NGC 2169 has a large low-mass population which potentially offers a more precise statistical investigation of several aspects of star formation and early stellar evolution. By modelling the distribution of low-mass stars in the I_C versus $R_C - I_C$ diagram, we find that any age spread among cluster members has a Gaussian full width at half-maximum (FWHM) $\leqslant$ 2.5 Myr. A young age and a small age spread (<10 Myr) are supported by the lack of significant lithium depletion in the vast majority of cluster members. There is no clear evidence for accretion or warm circumstellar dust in the low-mass members of NGC 2169, bolstering the idea that strong accretion has ceased and inner discs have dispersed in almost all low-mass stars by ages of 10 Myr.

Key words: stars: abundances – stars: late-type – stars: pre-main sequence – open clusters and associations: individual: NGC 2169.

1 INTRODUCTION

There are notably few well-studied clusters in the literature with ages between about 5 and 30 Myr. Yet, investigating the coeval populations in such clusters is vital for our understanding of (i) the lifetimes and subsequent evolution of high-mass (8–20 $\mathrm{M}_\odot$) main-sequence stars which contribute the majority of metal enrichment to the Universe; (ii) the evolution of circumstellar material, formation of planetary systems and loss of angular momentum in lower mass stars.

In this paper, we report the first results from the Keele–Exeter young cluster survey (KEY clusters) to find and characterize clusters with age 5–30 Myr. NGC 2169 (=C 0605+139) is a concentrated, but sparsely populated, young open cluster (class I3p; Ruprecht 1966) in the constellation of Orion, with an age of $\simeq$ 10 Myr and distance of $\sim$1 kpc [see Perry, Lee & Barnes (1978) and Section 2]. Using CCD photometry and intermediate-resolution spectroscopy, we have uncovered the low-mass ($0.1 < M/\mathrm{M}_\odot < 1.3$) pre-main-sequence (PMS) population of NGC 2169 and used isochronal fits to the high- and low-mass stellar populations and measurements of photospheric Li depletion to test evolutionary models, determine the cluster age and investigate the possibility of any age spread within the cluster. Armed with an age, we have investigated time-scales for the dispersal of gas and dust discs by comparing the low-mass stars of NGC 2169 with those in younger and older clusters.

This paper is organized as follows. Section 2 summarizes previous work on this cluster; Section 3 describes a new photometric survey (the results of which are provided in electronic form) used to identify candidate low-mass cluster members; Section 4 describes intermediate-resolution spectroscopy from the *Gemini* North telescope which is used to confirm candidate membership and study Li depletion; Section 5 compares constraints on the cluster age imposed by low-mass isochrones, Li depletion models and the evolutionary status of high-mass stars in the cluster; Section 6 deals with the spatial structure and mass function (MF) of the newly discovered low-mass population and Section 7 discusses the evidence for age spreads within the cluster and the evolution of circumstellar accretion. Our conclusions are presented in Section 8.

2 PREVIOUS STUDIES OF NGC 2169

There are several previous studies of the high-mass population in NGC 2169. Photoelectric photometry of the brighter candidate

⋆E-mail: rdj@astro.keele.ac.uk

Table 1. Literature evaluations of the age, distance and reddening of NGC 2169.

Authors	$E(B-V)$ (mag)	Intrinsic distance modulus (mag)	Age (Myr)	Notes
Sagar (1976)	0.18	9.60	<9	*UBV* photoelectric
Harris (1976)			<12	MK spectra
Abt (1977)	0.17 ± 0.03	10.9 ± 0.3		MK spectra
Perry et al. (1978)	0.20 ± 0.01	10.2 ± 0.1	<23	*ubvyβ* photoelectric
Delgado et al. (1992)	0.20	10.05	<16	*ubvyβ* photoelectric
Peña & Peniche (1994)	0.25 ± 0.02	9.7 ± 0.3	<50	*ubvyβ* photoelectric

cluster members is presented in Cuffey & McCuskey (1956, in the *PV* system), Hoag et al. (1961, *UBV*), Sagar (1976, *UBV*), Perry et al. (1978, *uvbyβ*), Delgado et al. (1992, *uvbyβ*) and Peña & Peniche (1994, *uvbyβ*). Harris (1976) and Abt (1977) have published spectral types on the Morgan–Keenan system for the brightest stars in the cluster, and more recently Liu, Janes & Bania (1989) conducted a radial velocity (RV) survey of nine bright A and B stars in the cluster, finding several spectroscopic binaries. A number of surveys for peculiar or variable stars have been conducted [see Jerzykiewicz et al. (2003) and references therein], and at least two candidate beta Cepheids and an A0V Si star have been identified.

For this paper, the important parameters are the cluster age, distance and reddening. Table 1 gives a summary of the conclusions reached by other authors. There is good agreement between photometric and spectroscopic determinations of the reddening and very little star-to-star dispersion [$\sigma_{E(B-V)} \leqslant 0.02$; Delgado et al. 1992]. There is less agreement in the cluster distance and age, primarily because of disagreement over which stars should be considered members of the cluster and which stars are binary systems, but also because of different calibrations of the main-sequence turn-off upon which the age estimates are based. As there are no obviously evolved stars apart from the binary system Hoag 1 (B2III; Abt 1977), these ages are inevitably upper limits. We prefer the estimates provided by Perry et al. (1978) and Delgado et al. (1992), which attempt to weed out field interlopers before estimating the cluster parameters. For the moment, we assume the cluster is less than 23 Myr old, is at a distance of $\simeq$1000 pc and has $E(B-V) = 0.20$, although these parameters are re-assessed in Section 5.

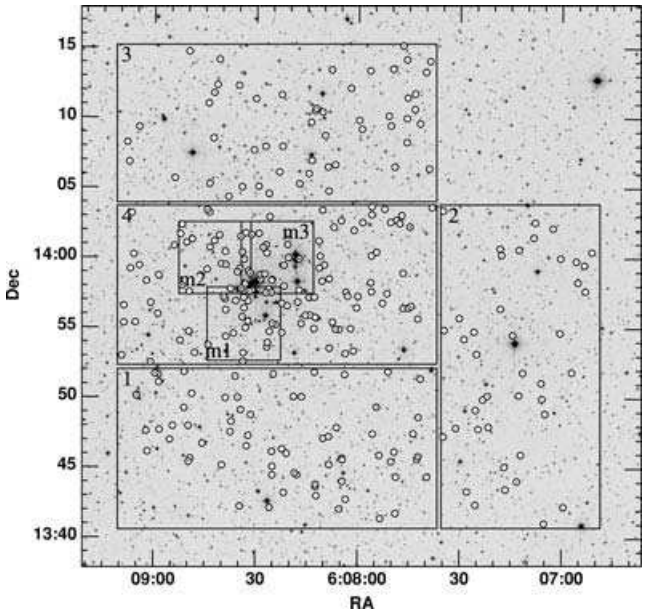

Figure 1. Location of the INT CCD and GMOS spectroscopic surveys. The large rectangles (labelled 1 to 4) show the individual detectors from the INT WFC (see Section 3). The small squares (labelled m1 to m3) show the three GMOS multislit masks (see Section 4.1). The small symbols mark the locations of photometric cluster candidates with $15.5 < I_C < 19.0$ (see Section 4.1).

3 CCD PHOTOMETRY OF NGC 2169

We observed NGC 2169 on the night beginning 2004 September 28, using the Wide-Field Camera (WFC). on the 2.5-m Isaac Newton telescope (INT). The camera consists of four thinned EEV (Chelmsford, UK) 2 k × 4 k CCDs (numbered 1–4) covering 0.33 arcsec pixel^{-1} on the sky. The arrangement of the four detectors on the sky for our observations of NGC 2169 is shown in Fig. 1. We obtained exposures in the Cousins *R* band (3, 30 and 3 × 350 s) and Sloan *i* band (2, 20 and 200 s). The night was photometric, and so we also obtained observations of standard stars from Landolt (1992) and Stetson (2000). Table 2 shows the range in colour of standards observed for each CCD.

Table 2. The range of colours for the photometric standards observed by each CCD detector.

CCD	Colour range
1	$0.340 < R_C - I_C < 1.839$
2	$0.318 < R_C - I_C < 1.750$
3	$0.342 < R_C - I_C < 2.323$
4	$0.207 < R_C - I_C < 2.314$

The data were de-biased and flat-fielded using master bias and master twilight sky flat frames. The *i*-band data were defringed using a library fringe frame. We extracted the NGC 2169 photometry using the optimal photometry techniques described in Naylor (1998) and Naylor et al. (2002). We first searched the sum of all three long *i*-band frames to produce a catalogue of objects, and then performed optimal photometry at the positions of these stars in all the frames. We flagged as 'I' (ill-determined sky) any stars which gave $\chi^2 >$ 3 when we fitted the distribution of counts in the sky (see Burningham et al. 2003). By comparing the measurements in the long *R* frames, we established that we should add a 1 per cent magnitude-independent uncertainty to measurements from a single frame. We included this when we combined the measurements to yield a single magnitude for each star in each filter, and at the same time flagged as variable any stars which had a reduced χ^2 of 10 or more compared with a constant value. The optimal photometry magnitudes were corrected to that of a large aperture using a spatially dependent aperture correction (see Naylor et al. 2002).

Table 3. The R_C versus $R_C - I_C$ photometric catalogue. This is a sample: the full table is available in the online version of this paper, in the Supplementary Material section, but a portion is shown here to illustrate its content. Columns list unique identifier: the right ascension and declination (J2000.0), the CCD pixel coordinates at which the star was found, and then for each of I_C and $R_C - I_C$ there is a magnitude, magnitude error and a flag [OO for a 'clean detection' – a detailed description of the flags is given by Burningham et al. (2003)].

Cat.	ID	RA	Dec.	x	y	I_C	δI_C	Flag	$R_C - I_C$	$\delta (R_C - I_C)$	Flag
		(J2000.0)				(mag)			(mag)		
1.04	206	06 08 32.011	+13 58 00.95	1075.155	1690.680	9.043	0.011	SS	1.016	0.014	SS
1.04	225	06 08 30.184	+13 57 32.44	1162.019	1769.860	9.222	0.011	SS	0.922	0.014	SS

Standard star photometry was also extracted using optimal photometry techniques and corrected to a larger aperture in the same way as the target data. The advantage of this over the more usual method of performing photometry directly in a large aperture was that we collected good signal-to-noise photometry on many more faint standards. The only disadvantage might be that some standards have been originally defined using a large aperture that included other objects. However, we note that our reduction process flags objects with photometry that is significantly perturbed by nearby companions and also that many of the fainter standards (from Stetson 2000) were in fact measured using PSF fitting in any case.

We fitted our standard star observations as a function of colour and airmass. The airmass range of our standard stars is small (1.1 to 1.3) and close to the airmass of our target observations (1.1), and so we fixed the extinction. Although a single linear relationship was sufficient to represent the conversion from instrumental i to I_C as a function of $R_C - I_C$, we found we had to use two separate linear relationships to convert instrumental $R - i$ to $R_C - I_C$, with the break occurring at $R_C - I_C = 1.0$ to 1.3 depending on CCD. We found that we needed to add a magnitude-independent uncertainty of 1 per cent in $R_C - I_C$ and 2 per cent in I_C (1.5 per cent if we just used the Landolt standards) to obtain a reduced χ^2 of unity. These values therefore correspond to the combined uncertainty in our profile correction, and our correction to the Cousins system. They are not included in the uncertainty estimates in our final catalogues, as they should not be added when comparing stars in a similar region of the CCD (see Naylor et al. 2002). We derived our astrometric calibration from Two-Micron All-Sky Survey (2MASS) stars (Skrutskie et al. 2006), with a rms of 0.1 arcsec for the fit of pixel position as a function of RA and Dec.

Our entire catalogue is presented as Table 3, which is available online, or from the Centre de Données astronomiques de Strasbourg (CDS) or from the 'Cluster' Collaboration's home page.[1] As an example of the data, Fig. 2 shows the I_C versus $R_C - I_C$ colour–magnitude diagram (CMD) for all unflagged (i.e. clean, star-like with good photometry) objects on CCD 4 with a signal-to-noise ratio (S/N) greater than 10. This CMD illustrates a clear PMS at the position in the CMD appropriate for a ∼10 Myr population at a distance of $\simeq$ 1000 pc. The sharp magnitude cut-off in Fig. 2 is an artefact of the signal-to-noise threshold we have placed on the plotted points. We judge our data to be almost complete down to this cut-off, although the catalogue detection limit is about 1 mag fainter. For the purpose of this paper (see Section 6), we only require that the data are substantially complete to $I_C = 19$ at $R_C - I_C \simeq 1.9$.

[1] http://www.astro.ex.ac.uk/people/timn/Catalogues/description.html

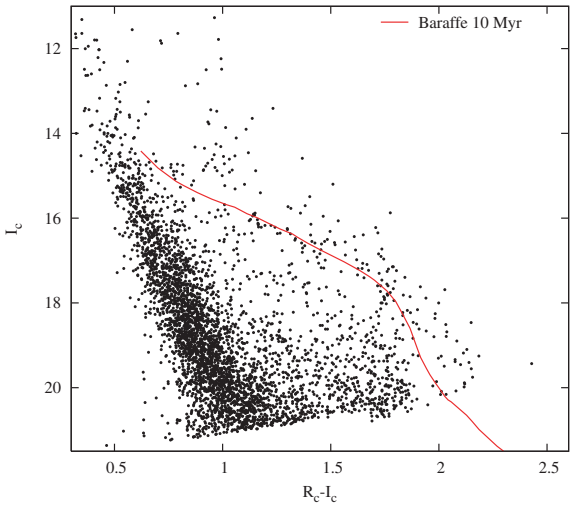

Figure 2. A CMD for unflagged objects with uncertainties < 0.1 mag in I_C and $R_C - I_C$ seen in CCD 4 (see Fig. 1). The solid line shows a theoretical 10 Myr PMS (from Baraffe et al. 2002) at an intrinsic distance modulus of 10.13, and with a reddening/extinction corresponding to $E(R_C - I_C) = 0.14$ (see Section 5).

4 *GEMINI* SPECTROSCOPY

4.1 Observations

The *Gemini* Multi-Object Spectrograph (GMOS) was used in conjunction with slit masks at the *Gemini* North telescope to observe 47 candidate low-mass members of NGC 2169 with $14.6 < I_C < 19.3$. This corresponds to a mass range (for an assumed distance of 1000 pc and an age of 10 Myr) of $0.14 < M/M_\odot < 1.3$ according to the models of Baraffe et al. (1998). Stars were targeted based on their location in the CMD and with the aim of maximizing the number of targets that could be included in three separate slit mask designs (see Table 4 and Fig. 1). Table 5 gives the coordinates and photometry of the targets, which are split according to the three masks they were observed in. One target (number 28) was observed in both mask 2 and mask 3.

Table 4. *Gemini* GMOS observation log giving the central position (telescope pointing) for each mask, the Julian Date at the observation midpoint, the number of targets in each mask, the exposure time and the average seeing.

Mask no.	RA	Dec.	Date	N	Exp time	Seeing
	J2000.0		(JD-245 3000)		(s)	(arcsec)
1	06 08 34.8	+ 13 55 12	672.108	18	3 × 1800	0.6
2	06 08 42.0	+ 14 00 00	706.973	15	3 × 1800	0.5
3	06 08 24.4	+ 14 00 00	674.100	15	3 × 1800	0.5

Table 5. Identification (as given in Table 3), positions and photometry for the 47 targets observed in three separate GMOS masks.

Target	Cat. ID		RA	Dec.	I_C	δI_C	$R_C - I_C$	$\delta\,(R_C - I_C)$
Mask 1								
01	1.04	1107	06 08 38.879	+13 54 22.45	17.189	0.009	1.626	0.011
02	1.04	1108	06 08 38.959	+13 56 15.66	17.462	0.010	1.736	0.009
03	1.04	1138	06 08 26.094	+13 54 44.42	17.303	0.009	1.724	0.012
04	1.04	1144	06 08 24.267	+13 55 13.57	17.187	0.009	1.645	0.011
05	1.04	1372	06 08 31.196	+13 57 40.47	16.520	0.008	1.334	0.010
06	1.04	1600	06 08 37.510	+13 57 47.18	18.002	0.012	1.733	0.014
07	1.04	1604	06 08 35.994	+13 56 54.98	18.142	0.012	1.731	0.013
08	1.04	170	06 08 41.962	+13 55 41.30	14.605	0.008	0.575	0.011
09	1.04	186	06 08 37.015	+13 52 43.91	15.608	0.007	0.784	0.009
10	1.04	1924	06 08 33.139	+13 54 59.24	18.519	0.014	1.834	0.017
11	1.04	214	06 08 32.212	+13 53 18.75	15.076	0.009	0.780	0.012
12	1.04	217	06 08 32.329	+13 57 00.56	14.893	0.009	0.773	0.011
13	1.04	252	06 08 26.809	+13 53 37.05	16.030	0.008	1.129	0.009
14	1.04	3039	06 08 33.925	+13 53 47.62	19.339	0.025	2.075	0.047
15	1.04	542	06 08 39.554	+13 57 12.76	16.171	0.008	1.196	0.009
16	1.04	555	06 08 34.112	+13 55 46.67	16.313	0.008	1.497	0.009
17	1.04	900	06 08 33.554	+13 56 24.88	17.093	0.009	1.668	0.011
18	1.04	903	06 08 32.401	+13 55 27.38	16.981	0.009	1.620	0.010
Mask 2								
19	1.04	1066	06 08 50.529	+14 01 05.12	17.340	0.009	1.624	0.011
20	1.04	1103	06 08 40.244	+13 59 33.45	17.261	0.009	1.761	0.009
21	1.04	1318	06 08 51.862	+14 02 21.58	17.597	0.010	1.731	0.013
22	1.04	1556	06 08 52.321	+14 01 40.77	18.228	0.013	1.833	0.015
23	1.04	159	06 08 43.331	+14 00 14.38	15.973	0.007	0.967	0.008
24	1.04	1610	06 08 34.387	+13 57 48.18	17.487	0.010	1.797	0.015
25	1.04	168	06 08 42.279	+14 01 11.94	15.905	0.007	1.026	0.008
26	1.04	195	06 08 35.413	+13 58 41.14	14.893	0.009	0.788	0.011
27	1.04	2269	06 08 35.533	+13 58 58.60	18.797	0.018	1.977	0.028
28	1.04	3044	06 08 33.238	+13 58 07.51	18.720	0.027	1.800	0.096
29	1.04	543	06 08 39.096	+14 00 26.21	16.270	0.008	1.300	0.009
30	1.04	552	06 08 34.845	+13 59 13.44	16.121	0.008	1.164	0.009
31	1.04	554	06 08 34.489	+14 01 31.66	16.394	0.008	1.650	0.009
32	1.04	718	06 08 33.516	+13 59 52.69	16.842	0.008	1.450	0.010
33	1.04	875	06 08 43.644	+14 00 44.47	16.964	0.009	1.745	0.010
Mask 3								
28	1.04	3044	Repeated in this mask					
34	1.04	906	06 08 28.739	+13 58 27.40	16.481	0.012	1.337	0.012
35	1.04	1154	06 08 19.214	+13 59 30.35	15.728	0.007	0.826	0.011
36	1.04	1367	06 08 33.076	+14 01 46.38	17.817	0.010	1.763	0.011
37	1.04	1622	06 08 32.337	+13 59 03.87	17.755	0.012	1.775	0.013
38	1.04	1641	06 08 26.254	+13 57 45.79	17.665	0.010	1.789	0.011
39	1.04	1947	06 08 27.496	+13 58 49.92	18.230	0.013	1.869	0.017
40	1.04	202	06 08 34.120	+14 00 24.11	15.955	0.008	1.465	0.009
41	1.04	224	06 08 31.387	+14 01 38.91	15.730	0.007	1.302	0.008
42	1.04	2349	06 08 17.379	+13 59 55.62	16.433	0.032	1.609	0.059
43	1.04	260	06 08 25.478	+14 02 11.90	14.866	0.009	1.045	0.011
44	1.04	2684	06 08 27.158	+13 57 29.07	18.685	0.017	2.037	0.029
45	1.04	563	06 08 28.518	+13 59 45.31	16.165	0.008	1.239	0.009
46	1.04	747	06 08 21.831	+13 57 58.72	16.551	0.008	1.413	0.009
47	1.04	929	06 08 20.784	+14 00 56.85	16.609	0.008	1.457	0.010

We used slits of width 0.5 arcsec and with lengths of approximately 8–10 arcsec. The R831 grating was used with a long-pass OG515 filter to block second-order contamination. The resolving power was 4400 and simultaneous sky subtraction of the spectra was possible. The spectra covered ∼2000 Å, with a central wavelength of 6200–7200 Å depending on the location of the slits within the 5.5 arcmin field of view.

Observations were taken in queue mode (program number GN-2005B-Q-30) through three separate masks during 2005 October and December (see Table 4). For each mask, we obtained 3×1800 s exposures bracketed by observations of a CuAr lamp for wavelength calibration and a quartz lamp for flat-fielding and slit location. The spectra were recorded on three 2048×4068 EEV chips leading to two $\simeq 16$ Å gaps in the coverage. The CCD pixels were binned 2×2

before readout, corresponding to ∼0.67 Å per binned pixel in the dispersion direction and 0.14 arcsec per binned pixel in the spatial direction. Conditions were clear with seeing of 0.5–0.6 arcsec [full width at half-maximum (FWHM) measured from the spectra].

The data were reduced using version 1.8.1 of the GMOS data-reduction tasks running with version 2.12.2a of the Image Reduction and Analysis Facility (IRAF). The data were bias-subtracted, mosaiced and flat-fielded. A two-dimensional wavelength calibration solution was provided by the arc spectra and then the target spectra were sky-subtracted and extracted using 2 arcsec apertures. The three individual spectra for each target were then combined using a rejection scheme which removed obvious cosmic rays. The instrumental wavelength response was removed from the combined spectra using observations of a white dwarf standard to provide a relative flux calibration. The same calibration spectrum was used to construct a telluric correction spectrum. A scaled version of this was divided into the target spectra, tuned to minimize the rms in regions dominated by telluric features.

The S/N of each combined extracted spectrum was estimated empirically from the rms deviations of straight line fits to segments of 'pseudo-continuum' close to the Li I 6708 Å features (see below). As small unresolved spectral features are expected to be part of these pseudo-continuum regions, these S/N estimates, which range from ∼10 to 20 in the faintest targets to >200 in the brightest, should be lower limits. Examples of the reduced spectra are shown in Fig. 3. All the reduced spectra are available in 'fits' format from the 'Cluster' Collaboration's home page (see footnote 1).

4.2 Analysis

Each spectrum was analysed to yield a spectral type, equivalent widths (EWs) of the Li I 6708 Å and Hα lines and a heliocentric RV. Each of these analyses is described below. The results are given in Table 6.

4.2.1 Spectral types

Spectral types were estimated from the strength of the TiO(7140 Å) narrow-band spectral index (see Oliveira et al. 2003). This index is quite temperature sensitive and can be calibrated for spectral type using spectra of well-known late K- and M-type field dwarfs. We constructed a polynomial relationship between spectral type and the TiO(7140 Å) index that was used to estimate the spectral type of our targets, based on a numerical scheme where M0–M6 = 0–6, K5 = −2 and K7 = −1. Table 7 gives the adopted relationship between the TiO(7140 Å) index and spectral type. The scatter around the polynomial indicates that these spectral types are good to ± half a subclass for stars of type M0 and later, but to only a subclass at

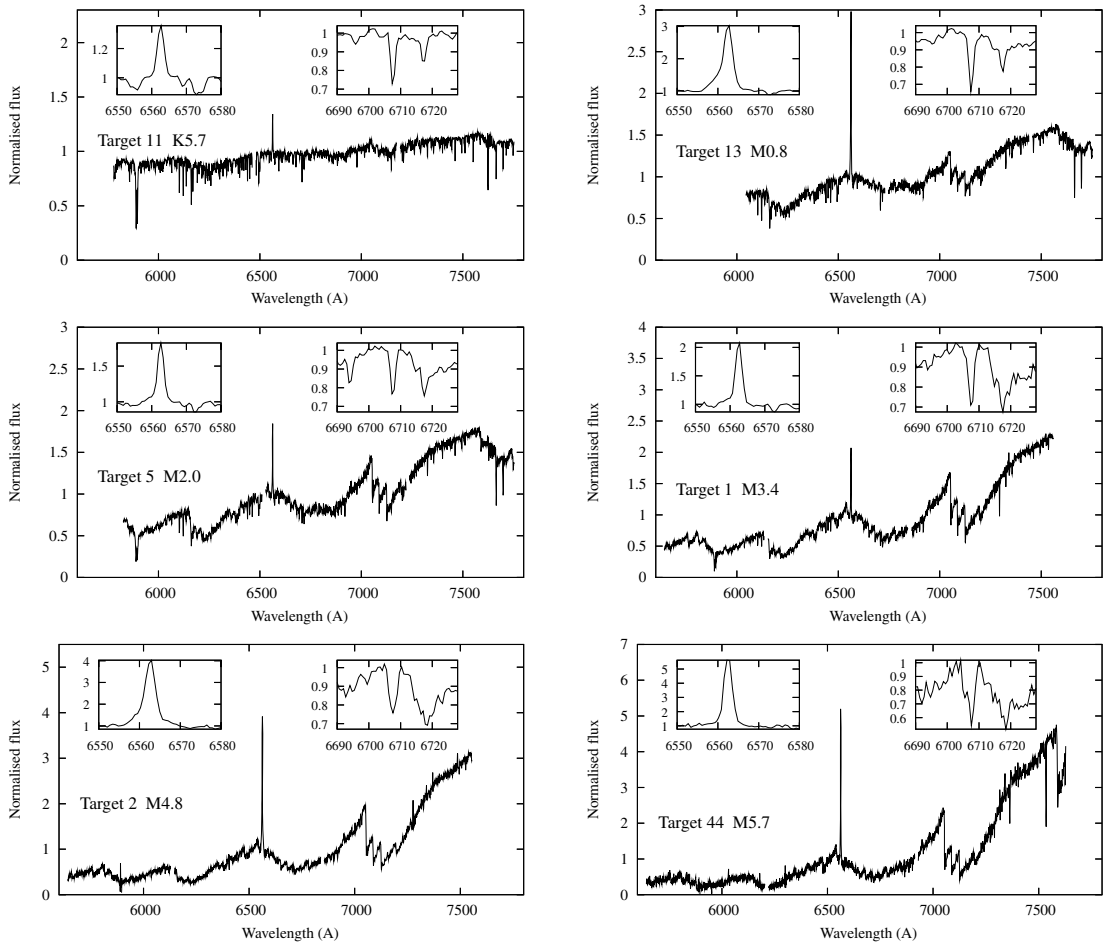

Figure 3. Example spectra from our target list, covering the full range of spectral type and S/N. Spectra have been subjected to relative flux calibration and telluric correction, and have been normalized to a continuum point near Hα. The inserts on each plot show normalized spectra in the regions of the Hα and Li I 6708 Å lines.

Table 6. Results from the spectral analysis of Section 4.2, listing spectral type, estimated S/N, EWs of the Li I 6708 Å and Hα lines and the heliocentric RV. The last column gives the overall membership assessment – Y member, N non-member, ? membership questionable (see Section 4.3).

Target	Spectral type	S/N	EW(Li) (Å)	δEW(Li) (Å)	FWHM(Li) (Å)	EW(Hα) (Å)	RV (km s^{-1})	δRV (km s^{-1})	Mem?
Mask 1									
01	M3.4	77	0.62	0.02	1.86	−3.0	11.7	1.8	Y
02	M4.8	41	0.68	0.05	2.54	−12.1	16.6	5.5	Y
03	M4.2	45	0.50	0.04	1.86	−4.3	14.4	2.8	Y
04	M3.7	95	0.52	0.02	1.74	−3.7	15.1	2.2	Y
05	M2.0	100	0.45	0.02	1.65	−2.1	11.7	0.2	Y
06	M4.7	37	0.63	0.04	1.97	−5.4	12.6	3.2	Y
07	M4.4	23	<0.24	–	–	−0.1	−33.0	3.6	N
08	K5.3	180	<0.03	–	–	−1.7	29.9	16.7	?
09	K5.6	220	<0.03	–	–	+0.5	−27.2	5.0	N
10	M5.3	16	0.67	0.09	1.57	−5.7	14.7	3.8	Y
11	K5.7	156	0.47	0.01	1.53	−0.9	24.5	8.8	Y
12	K5.7	212	0.52	0.01	2.35	−1.3	19.4	6.1	Y
13	M0.8	108	0.59	0.01	1.62	−6.6	8.5	1.7	Y
14	M5.5	8	<0.68	–	–	−18.8	18.3	3.8	?
15	M1.1	133	0.52	0.01	1.62	−2.5	8.7	2.0	Y
16	M2.8	76	0.56	0.02	1.79	−8.9	13.7	2.2	Y
17	M3.5	67	0.54	0.02	1.81	−3.6	14.9	2.4	Y
18	M3.7	52	0.63	0.03	1.74	−3.3	16.4	1.7	Y
Mask 2									
19	M3.4	86	0.49	0.02	1.86	−1.1	14.1	5.7	Y
20	M4.9	48	0.61	0.03	1.76	−1.2	20.1	3.3	Y
21	M4.2	27	< 0.20	–	–	–	27.9	3.9	N
22	M5.0	32	0.84	0.06	3.12	−9.4	16.3	8.5	Y
23	K7.3	111	<0.05	–	–	+0.9	−36.5	3.4	N
24	M4.2	40	0.64	0.04	2.26	−4.8	14.4	2.6	Y
25	K7.7	173	0.53	0.01	1.69	−1.7	9.3	3.3	Y
26	K5.9	266	0.47	0.01	1.41	−1.3	12.1	3.5	Y
27	M5.6	20	0.71	0.07	1.34	−13.6	25.0	6.4	Y
28	M5.3	14	0.98	0.14	2.84	−10.4	20.4	4.2	Y
29	M1.4	78	0.57	0.02	1.71	−6.4	10.5	1.7	Y
30	M0.5	80	–	–	1.97	−3.5	8.4	1.8	?
31	M3.7	53	0.54	0.03	1.81	−6.7	13.4	2.3	Y
32	M3.0	61	0.37	0.02	1.67	−3.5	13.4	1.4	Y
33	M4.0	39	0.56	0.04	1.65	−5.9	12.8	2.7	Y
Mask 3									
28	M5.3	20	1.07	0.09	2.32	−7.9	17.8	8.1	Y
34	M2.2	75	0.54	0.02	1.65	−3.8	12.1	2.0	Y
35	K5.9	126	<0.05	–	–	+0.6	−53.3	2.3	N
36	M4.9	55	0.59	0.03	1.69	−5.7	15.9	5.9	Y
37	M5.0	41	0.71	0.04	1.81	−7.3	18.7	5.3	Y
38	M4.7	25	0.61	0.06	1.79	−6.6	18.8	3.5	Y
39	M5.0	35	0.63	0.06	2.84	−6.2	21.4	4.5	Y
40	M3.0	92	0.62	0.02	2.02	–	6.4	5.3	Y
41	M1.7	87	–	–	–	−4.4	4.0	3.4	?
42	M3.8	46	–	–	–	−5.8	26.7	2.4	?
43	K5.1	134	<0.04	–	–	+1.5	27.4	6.9	N
44	M5.7	17	1.10	0.12	3.17	−11.7	18.3	4.5	Y
45	M1.8	76	0.59	0.02	1.57	−3.7	12.4	1.9	Y
46	M2.6	123	0.61	0.01	1.81	−2.6	17.5	1.4	Y
47	M1.8	61	0.58	0.03	1.72	−2.3	16.6	0.9	Y

earlier type stars as the molecular band is very weak at spectral type K5.

A plot of spectral type derived from the TiO(7140 Å) index versus $R_C - I_C$ colour reveals a smooth relationship (see Fig. 4) with little scatter. We expect this even if there is some contamination by field interlopers in the sample. These would have similar colours and spectral types to the cluster members, but would be foreground objects with lower luminosities. A comparison of the positions of standard stars on this plot ($R_C - I_C$ colours where available are from Leggett 1992) reveals an average redward offset of $\simeq 0.05$ mag in

Table 7. The relationship between TiO(7140 Å) index and spectral type.

Index	Spectral type
0.99	K5
1.13	K7
1.26	M0
1.40	M1
1.53	M2
1.74	M3
2.08	M4
2.61	M5
3.38	M6

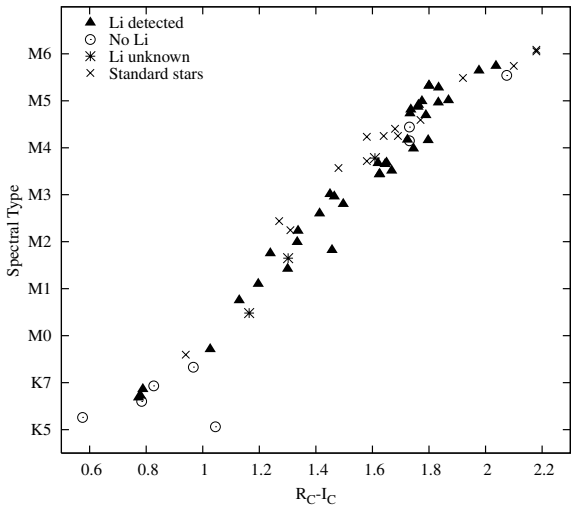

Figure 4. Spectral types deduced from the TiO(7140 Å) index as a function of $R_C - I_C$. Also shown are results from the spectra of standard stars where $R_C - I_C$ is available (see text).

the $R_C - I_C$ values of our targets at a given spectral type. Of course, we expect cluster members to have suffered a reddening $E(R_C - I_C) \simeq 0.14$ mag [corresponding to $E(B - V) = 0.20$ mag; Taylor 1986]. This comparison demonstrates that the photometric calibration for these red stars is reasonable, although there is a hint that the $R_C - I_C$ values may be too blue at the reddest colours. We have to temper this conclusion with the probability that the relationship between colour and spectral type is slightly different in very young stars.

4.2.2 Lithium measurements

The Li I 6708 Å resonance feature should be strong in cool young stars with undepleted Li – with an EW of 0.5 to 0.6 Å according to the curves of growth presented by Zapatero Osorio et al. (2002). Insets in Fig. 3 show the Li region in a number of our targets. Lithium is an ephemeral element in the atmospheres of very cool stars, and its presence in the photospheres of late K- and M-type stars is a strong indicator of youth.

The EW of the Li I 6708 Å feature was estimated by fitting it with a Gaussian function. We preferred this to direct integration because in lower signal-to-noise spectra, we eliminate the subjectivity involved in choosing the integration limits and we get a straightforward indication of rapid rotation (see below). The 'pseudo-continuum' was estimated using straight line fits to the regions immediately around the Li feature, excluding regions beyond 6712 Å which contain a strong Ca line and which are noisy due to the subtraction of a strong S II sky line. None of the Li lines in our spectra shows any strong evidence for a non-Gaussian shape or double lines; target 44 (shown in Fig. 3) has the most 'non-Gaussian' appearance, but even here the Gaussian fit is only rejected at 93 per cent confidence and in any case the EW estimated by direct integration would not differ significantly from the Gaussian result. The EW and Gaussian FWHM of the Li lines are given in Table 6. Uncertainties in the EW are estimated using the formula $\delta\,\mathrm{EW} = \sqrt{2fp}/\mathrm{S/N}$, where $2f$ is twice the Gaussian FWHM of the line (approximately the range over which the EW is integrated) and p is the pixel size (0.67 Å).[2] In eight cases, there was no obvious Li feature to measure, in which case a 3σ upper limit is quoted. In three cases, the Li feature fell in a gap between the detectors, and no EW could be measured.

For the majority of the sample, there are clear detections of the Li feature with EW > 0.3 Å. Comparisons with Li depletion patterns in open clusters of known age (e.g. see fig. 10 of Jeffries et al. 2003) place empirical age constraints on these stars. Li EWs of > 0.3 Å are not seen for any stars of spectral type cooler than K5 in the Pleiades or Alpha Per clusters (with ages of 120 and 90 Myr, respectively, and excepting the very low luminosity stars beyond the lithium depletion boundary where Li remains unburned – see Soderblom et al. 1993; Jones et al. 1996). Nor can strong Li lines be seen in M dwarfs of the 35–55 Myr open clusters NGC 2547, IC 2391 and IC 2602 (see Randich et al. 2001; Jeffries et al. 2003; Barrado y Navascués, Stauffer & Jayawardhana 2004; Jeffries & Oliveira 2005, and again excepting the very cool M dwarfs beyond the lithium depletion boundary). In summary, we assume that objects with EW[Li] > 0.3 Å are all younger than 100 Myr and younger than 50 Myr if they have spectral type $\geqslant$M0. These Li-rich objects are therefore very likely to be members of NGC 2169, and this conclusion is supported by RV measurements (see below). However the converse may not be true – a lack of Li is not used as the sole criterion for excluding a candidate member, as one of the aims of this paper is to investigate possible instances of anomalously large Li depletion.

In a number of cases, the FWHM of the Li I 6708 Å line is significantly broader than the 1.7 Å expected from the intrinsic width of the doublet and the instrumental resolution. In these cases, rotational broadening is suspected, which implies projected rotational velocities from 25 km s^{-1} (for a FWHM of 2 Å) to 60 km s^{-1} for the broadest lines.

4.2.3 Hα measurements and circumstellar material

Hα EWs were measured for all our targets (except two where the feature fell in a detector gap) by direct integration above (or below) a pseudo-continuum. The main uncertainty here is the definition of the pseudo-continuum as a function of spectral type and probably results in uncertainties of the order of 0.2 Å, even for the bright targets.

Hα emission is ubiquitous from young stars. It either arises as a consequence of chromospheric activity or is generated by accretion activity in very young objects (e.g. Muzerolle, Calvet & Hartmann 1998). The Hα emission from accreting 'classical' T-Tauri

[2] This formula arises from adding the uncertainties in each pixel flux estimate in quadrature, assuming that these uncertainties are given by the average S/N and that the line is integrated over a range of $2f$. The additional statistical uncertainty due to the continuum level estimate is small in comparison.

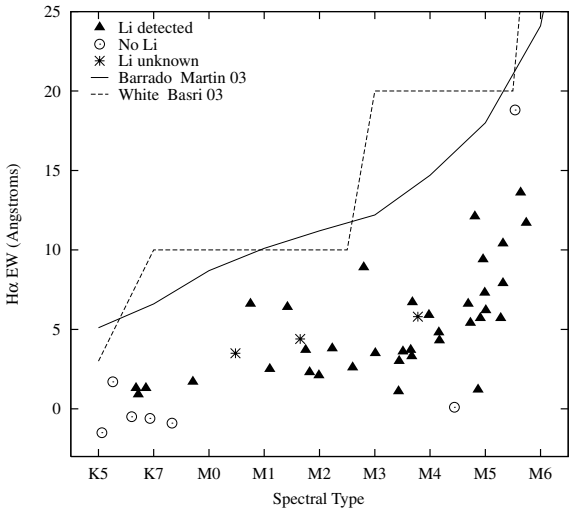

Figure 5. Hα EW as a function of spectral type. Objects with Li, without Li or where the Li status is unknown are indicated. Two lines are shown that have previously been used to separate accretion-generated Hα emission from a lower level of emission that could be attributable to a chromosphere (Barrado y Navascués & Martín 2003; White & Basri 2003).

stars (CTTS) is systematically stronger and broader (velocity widths >270 km s^{-1}; White & Basri 2003) than the weak line T-Tauri stars (WTTS) where the emission is predominantly chromospheric.

An empirical division between CTTS and WTTS can be made on the basis of either Hα EW or the width of the Hα emission line (e.g. Barrado y Navascués & Martín 2003; White & Basri 2003). Fig. 5 shows the Hα EW of our targets (where available) versus spectral type along with the empirical dividing line between CTTS and WTTS defined by Barrado y Navascués & Martín and by White & Basri. On the basis of these plots, none of our targets are clear examples of CTTS. A caveat here is that we have a single epoch spectrum. Accretion or chromospheric activity can be variable phenomena, and multiple observations are preferable for a secure classification. Large variations in Hα strength have been seen in some PMS stars (e.g. Littlefair et al. 2004), however in a recent paper by Jayawardhana et al. (2006), multiple Hα spectra did not reveal variability that would change the classification of a significant fraction of young objects. The most likely error would be a chromospheric flare leading to a CTTS classification for a WTTS.

The profiles of the Hα line were inspected for all targets and apart from targets 8 and 13, none shows evidence for velocity widths (at 10 per cent of maximum) in excess of 300 km s^{-1}. Target 8 is discussed in Section 4.3, it does not show a Li I 6708 Å line and is probably not a cluster member. Target 13 (shown in Fig. 3) has a narrow, strong Li I line and shows a blue Hα emission wing extending to $\sim$200 km s^{-1}. The Hα EW lies below the accretion thresholds in Fig. 5. It is possible that either accretion at a low level or chromospheric flaring could explain this observation. There are a number of other objects with widths at about the 270 km s^{-1} threshold advocated by White & Basri (2003) as an accretion discriminator. However, we note that our spectral resolution (70 km s^{-1} FWHM) is relatively poor compared to that used by White & Basri. That and the fact that some objects appear to have rotationally broadened photospheric Li lines mean that this threshold should be raised considerably in some cases. None of the targets shows any evidence for other emission lines that are often (but not always) associated with young accreting low-mass stars, such as He I 5876, 6678 Å.

In addition, we have checked for any emission from warm circumstellar dust by plotting the $H-K$ versus I_C-J colour–colour diagram (see Fig. 6a). *JHK* photometry for our targets was taken from the 2MASS point source catalogue (Skrutskie et al. 2006). An excess would show up as an anomalously large $H-K$ colour with respect to the photospheres of dwarf stars with the same I_C-J, although $H-K$ is nowhere near as sensitive to warm dust as excesses at longer wavelengths. None of our targets is significantly (>2 sigma) discrepant from the main-sequence dwarf locus reddened according to $E(B-V)=0.2$. The same is true of the more conventional $J-H$ versus $H-K$ diagram (Fig. 6b). In summary, we find no strong evidence for accretion or warm circumstellar dust in any of our targets.

4.2.4 Radial velocities

Our observations were not optimized for measuring RVs – minimal arc calibrations were performed and no RV standards were observed.

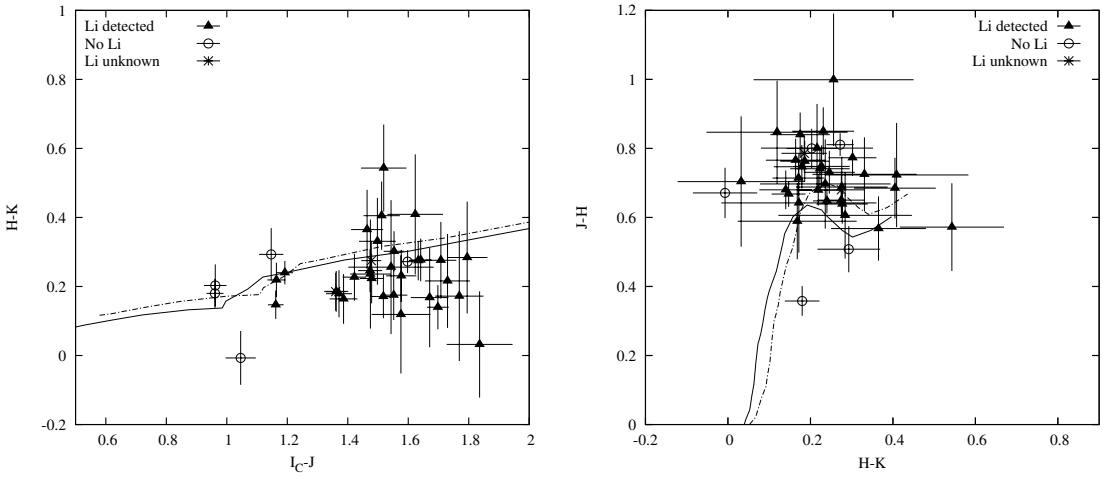

Figure 6. Near-infrared colour–colour diagrams for candidate members of NGC 2169. Objects with Li, without Li or where the Li status is unknown are indicated. The data plotted are our own I_C magnitudes combined with *JHK* magnitudes from 2MASS (Skrutskie et al. 2006). Only points with uncertainties lower than 0.2 mag in each colour are shown. Solid lines show the intrinsic loci of main-sequence dwarfs (from Bessell & Brett 1988). Dashed lines show the effects of reddening corresponding to $E(B-V)=0.20$, using the reddening law of Rieke & Lebofsky (1985).

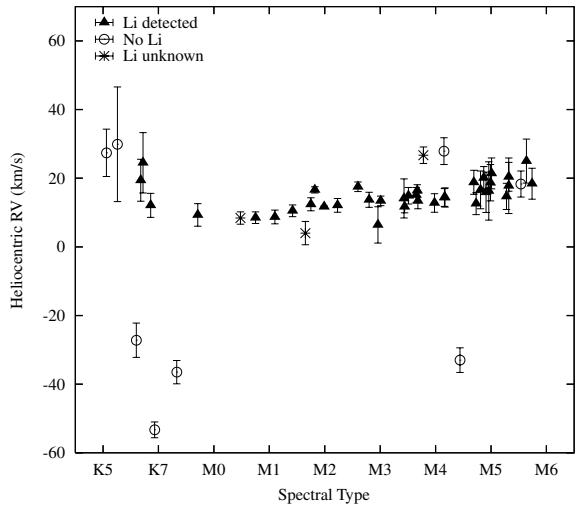

Figure 7. Radial velocities as a function of spectral type. Stars with and without Li and those with unknown Li status are indicated.

Nevertheless, we have been able to estimate RVs of all the targets relative to *one* of the targets and then estimate a zero-point based on archival spectra.

Relative RVs were determined by cross-correlation against target 5. We chose this star to act as a template because it has a high S/N and with a spectral type of M2, it has spectral features in common with targets of both earlier and later spectral types.

A correlation wavelength range of 6600–7400 Å was used for stars of spectral type M0 and later. For earlier spectral types where molecular features become small, the range 6000–6500 Å was used. Raw correlation lags were adjusted to the same heliocentric reference frame. A further correction to the RV zero-point was estimated by cross-correlating sky emission lines between the target spectra and the spectrum of target 5 *prior* to the sky subtraction data-reduction step. The typical size of this correction was $\pm$ 3 km s^{-1}, reflecting inaccuracies in the wavelength calibration, possibly due to flexure in the spectrograph during the 90 min of observation for each mask. A heliocentric RV zero-point was estimated by cross-correlating stars of type M4 or later with archival VLT UV–Visual Echelle Spectrograph (UVES) spectra of the M4V–M6V stars GL 402, 406 and 876 for which precise heliocentric RVs are known (see Bailer-Jones 2004 for details).

Heliocentric RVs versus spectral type are plotted in Fig. 7. Typical internal uncertainties are of the order of a few km s^{-1}. Most objects are closely clustered in this diagram. However, there is a clear upward trend towards later spectral types that seems to be a consequence of spectral type mismatch between target and template, probably due to our reliance on broad molecular bands rather than on sharp atomic lines in the later-type stars. Our best estimate for the true heliocentric RV of the cluster is $+16.8 \pm 1.1$ km s^{-1} from the Li-rich stars of spectral type M4 or later. The quoted error includes the scatter in our measurements and an estimate of the external uncertainty judged from the variance of results using the three different standard star templates. Our result agrees with (though is much more precise than) the $+16.6 \pm 6.0$ km s^{-1} quoted by Rastorguev et al. (1999).

4.3 Cluster membership

The presence of a strong (EW > 0.3 Å) Li I 6708 Å feature is taken as a positive indicator of membership and is entirely supported by the chromospheric Hα emission exhibited by all these Li-rich objects. The Li-rich candidates also have RVs with a very small intrinsic dispersion (less than a few km s^{-1} after taking account of the broad trend with spectral type) that is consistent with cluster membership.

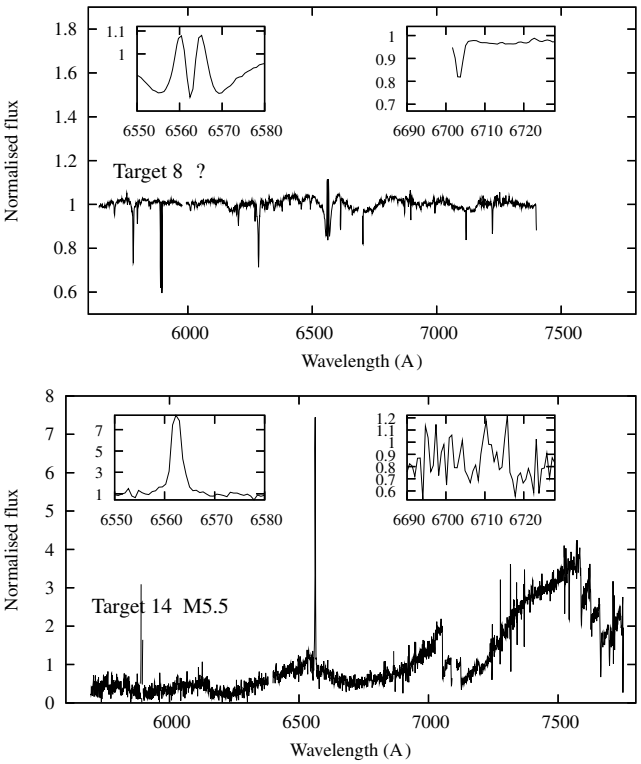

Figure 8. Spectra for two targets with questionable cluster membership (see Section 4.3). The inserts show normalized regions around the Hα and Li I features.

All three of the M dwarfs with no Li measurement have Hα emission lines consistent with the Li-rich targets. However, Hα emission is no guarantee of extreme youth among M dwarfs, and one of these three objects has a RV inconsistent with cluster membership, unless it is a short period binary system. For now, we regard all three objects as questionable members.

In order to investigate the possibility of anomalously large Li depletion, we also consider those targets where Li was undetected. Of eight such targets, five have an Hα line in absorption or barely in emission. These are extremely unlikely to be young objects and all have a RV which is inconsistent with cluster membership. These five are all classified as definite non-members. One object has no Hα measurement and a RV inconsistent with cluster membership, and we also classify this as a definite non-member. The remaining two objects have unusual spectra (see Fig. 8) which are discussed below.

Target 8. This star shows double-peaked central Hα emission within a broad absorption feature. The spectrum is dominated by several strong absorption lines at 5780.5, 5796.9, 6283.9, 6613.7 and 7224.0 Å, which can be identified with diffuse interstellar absorption bands (DIBS). There is no Li at 6708 Å although there is an unidentified line at 6703 Å. The EWs of the DIBS imply quite a high reddening. Using the relationships given by Jenniskens & Desert (1994), we estimate $E(B-V) \simeq 0.9$. From this, and also from the position of the star in the $J-H$ versus $H-K$ diagram, we infer that it has a spectral type of late A or early F and that the spectral type of K5 assigned in Section 4.2.1 must be in error. The star

lies bluewards of the best-fitting cluster isochrone in the I_C versus $R_C - I_C$ CMD, and the presence of additional reddening would increase this discrepancy. However, given that the Hα emission profile strongly suggests circumstellar material and possibly an accretion disc, we cannot be sure that the intrinsic optical colours would be representative of the photosphere of a late A star in any case. Hence, this object could be a young Herbig Ae star either within NGC 2169 or more likely at a much greater distance. Given this uncertainty, we will not consider the star as a cluster member in what follows.

Target 14. This object has an upper limit to its Li EW which could just be consistent with the presence of significant Li in the photosphere. Indeed, there is a hint of a Li line at the 1–2 sigma level. Its EW[Hα] is the largest in our sample and close to the empirical border between CTTS and WTTS. Its RV is consistent with cluster membership. The width of the Hα line is only $\simeq$180 km s^{-1} at 10 per cent of maximum. The status of this star is questionable. It is either a cluster member or a very active foreground dMe star. A better spectrum of the Li I 6708 Å line is needed and it is not considered as a cluster member in the analysis that follows.

5 AGE ESTIMATES

Absolute ages for open clusters are usually model dependent. This is especially true in very young open clusters and star-forming regions. A valuable exercise is to compare cluster ages derived from techniques that rely on different aspects of stellar physics. Agreement would instil confidence in the accuracy of stellar ages whilst discrepancies would highlight potential weaknesses in our understanding of stellar evolution.

Previous work has taken ages determined by fitting model isochrones to the positions of high-mass stars that have undergone nuclear evolution in the Hertzsprung–Russell (HR) diagram, and compared them with ages determined from isochrones which trace the descent of low-mass PMS stars contracting towards the hydrogen burning main sequence. In clusters with ages of 50–700 Myr, good agreement has been claimed (e.g. Lyra et al. 2006), but in younger clusters (<30 Myr) discrepancies are more common (e.g. Piskunov et al. 2004). Here, ages from evolved high-mass stars are often more uncertain because there are fewer such objects and the ages are dependent on details such as rotation and the degree of mixing in the convective core (Chiosi, Bertelli & Bressan 1992; Meynet & Maeder 1997, 2000). The ages obtained from fitting low-mass isochrones also become more model dependent – the details of the stellar atmospheres, interior convection and even the initial conditions become increasingly important (see Baraffe et al. 2002).

A third technique has begun to be added to these comparisons. The abundance of Li in convective envelopes and atmospheres is sensitively dependent on the temperature at the base of the convection zone (or stellar centre in the case of fully convective PMS stars). Once at a threshold temperature of about 3×10^6 K, Li is burned rapidly in (p, α) reactions. The mass, and hence luminosity and temperature at which Li burning commences, is age dependent and isochrones of Li depletion can be used to estimate the ages of clusters [see Jeffries (2006) for a review]. This technique has been used to obtain precise ages for several open clusters. Isochronal ages from high-mass stars agree with the lithium depletion ages for open clusters in the range 50–150 Myr provided that some extra mixing (caused by core overshoot or rotation?) extends the main-sequence lifetimes of 5–8 M$_\odot$ stars (Stauffer, Schultz & Kirkpatrick 1998; Stauffer et al. 1999; Barrado y Navascués et al. 2004). Jeffries & Oliveira (2005) have also shown that the lithium depletion age of a 35 Myr cluster agrees with an age derived from isochronal fits to low-mass PMS stars in the same cluster. However, discrepancies have also been reported. Song, Bessell & Zuckerman (2002) and White & Hillenbrand (2005) have reported on individual PMS stars which appear to show much more Li depletion than expected for their isochronal ages in the HR diagram.

5.1 Isochrone matches to high-mass stars

The high-mass population of NGC 2169 is relatively sparse with only one clearly evolved B2 III binary star (Abt 1977). Age constraints from these stars will therefore be quite poor, but we can still get valuable constraints on the cluster distance that will be useful when considering low-mass isochronal fits. Perry et al. (1978) based their age on what they consider to be the brightest, unevolved, non-binary member of NGC 2169 – namely Hoag 6, with a spectral type of B3V (Abt 1977). A calibration of the duration of main-sequence burning and absolute magnitude due to Schlesinger (1972) was used, leading to an upper age limit of 23 Myr. Delgado et al. (1992) claim a similar status for Hoag 4 with a spectral type of B2.5IV (Abt 1977) or B2V (Harris 1976) and hence determine a slightly lower upper age limit of 16 Myr.

We have re-evaluated the reddening, distance and age of NGC 2169 using the *UBV* data set published by Sagar (1976) together with the solar metallicity evolutionary models of Schaller et al. (1992) which have been transformed into isochrones in the Johnson *UBV* system by Lejeune & Schaerer (2001, henceforth known as the Geneva models and isochrones). The Sagar (1976) data set is the largest homogeneous set of photoelectric data for NGC 2169. We reviewed the cluster membership using information in Sagar (1976), Perry et al. (1978) and Delgado et al. (1992). There was generally consensus over membership, but in three cases (Hoag 2, 5 and 15) membership is disputed.

The intrinsic $U - B$ versus $B - V$ colour–colour diagram, V versus $B - V$ and V versus $U - B$ CMDs are shown in Fig. 9. We find that a reddening of $E(B - V) = 0.20 \pm 0.01$ applied to the 10 Myr Geneva isochrone satisfactorily models the colour–colour diagram. Note that we only consider the age-independent main-sequence portion of the $U - B$ versus $B - V$ diagram below the 'blue turn-off' and exclude the bluest (evolved) star from the fit. As this portion of the colour–colour locus is age independent for ages $\leqslant$20 Myr, the reddening estimate is also independent of assumed age in this range (see below). Then, assuming that $A_V/E(B - V) = 3.10$, the V versus $B - V$ CMD can be matched (by eye) with an intrinsic distance modulus of 10.2 ± 0.2. From this CMD, the age of the cluster is certainly less than 20 Myr based on the two brightest undisputed members and could be less than 10 Myr based only on the brightest object. The brightest star in the cluster is actually a close-to-equal mass binary system but this does not affect the age limit because the 10 Myr isochrone is almost vertical at this magnitude. In principle, V versus $U - B$ could offer better distance precision because the ZAMS locus has a shallower gradient for B stars in this CMD. However, we find the photometry appears more scattered, with points lying well outside a plausible band that could be explained by equal-mass binary systems. In this CMD, a less certain distance modulus of 10.2 ± 0.3 and an age of $\simeq$10 Myr seem appropriate. An age of $\geqslant$ 20 Myr or more is still ruled out by the brightest pair of undisputed members.

To put the distance estimate on a firmer basis, we fitted the V versus $B - V$ data using the τ^2 technique described in detail by Naylor & Jeffries (2006). τ^2 is a generalization of χ^2 that can be used to fit data points to a two-dimensional distribution, hence allowing for the binary content of a cluster sequence in the CMD, and provides

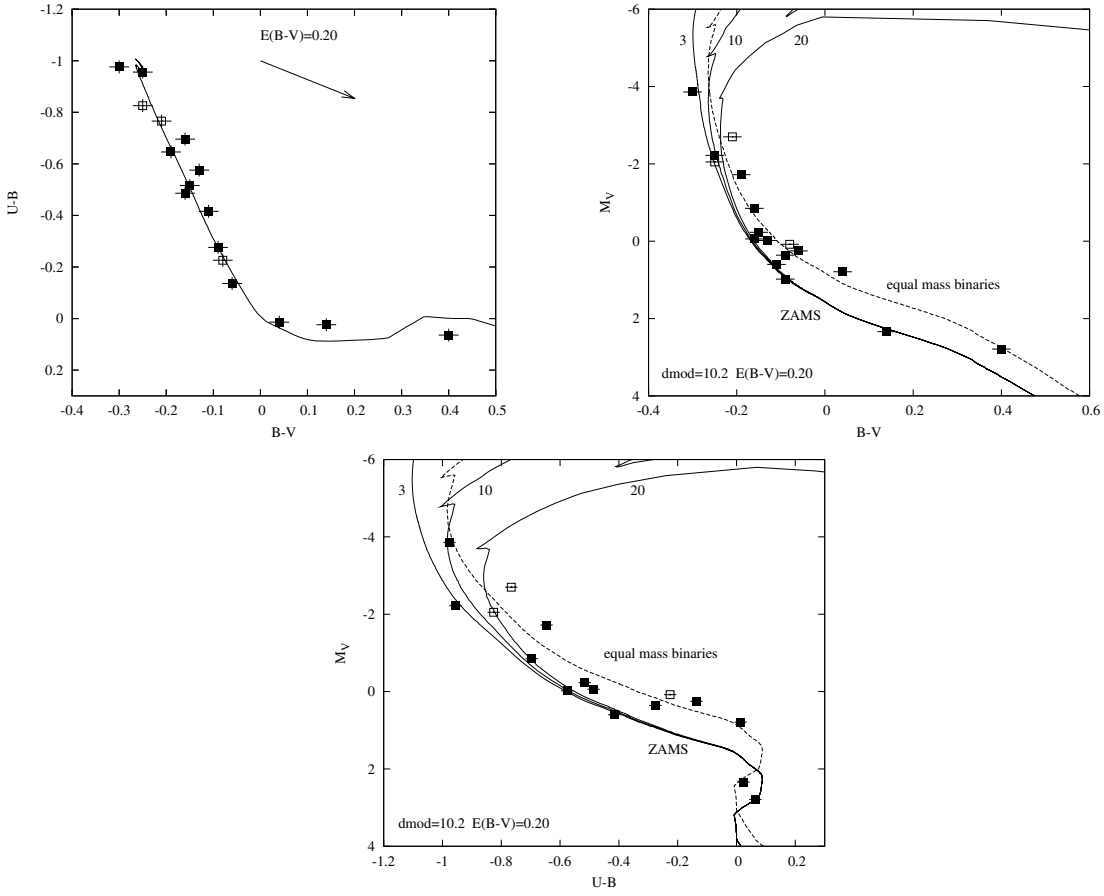

Figure 9. The intrinsic colour–colour and colour–magnitude diagrams for early-type members of NGC 2169. Data from Sagar (1976) are plotted. Open symbols indicate objects whose membership status is uncertain or disputed. Geneva model isochrones are from Lejeune & Schaerer (2001). (a) A 10 Myr isochrone is plotted after a reddening of $E(B-V) = 0.20$ and $E(U-B) = 0.146$ has been subtracted from the data. (b) and (c) Isochrones with ages of 3, 10 and 20 Myr are shown. The additional dashed line indicates the equal-mass binary sequence for the 10 Myr isochrone.

robust, statistically meaningful error bars. We assumed that a 10 Myr Geneva isochrone was appropriate and a binary fraction of 50 per cent, with secondary stars in the binaries randomly selected from a uniform mass distribution between the mass of the primary and zero. As discussed in Naylor & Jeffries (2006), the precise value of the binary fraction has only a small impact on the derived parameters. In this case, the intrinsic distance modulus of the cluster was the only free parameter, and we fitted to all data points apart from the brightest, Hoag 1, in order to ensure that the derived distance was insensitive to the assumed age.[3] We searched in distance modulus, to yield the τ^2 plot shown in Fig. 10 and a best-fitting distance modulus of 10.13 (in reasonable agreement with the 'by-eye' result above), with a 68 per cent confidence range of 10.04–10.19 (see Table 8). The data and best-fitting model are shown in Fig. 11. We obtained a $P_r(\tau^2)$ (equivalent to the probability of exceeding a given χ^2) of 0.03, indicating that the model just about provides a satisfactory representation of the data and that the uncertainties are approximately correct. Adding a systematic error of 0.02 mag to each data point would bring $P_r(\tau^2)$ up to 0.5, increasing the distance modulus uncertainty only slightly.

[3] In fact, we attempted a search for the best-fitting distance *and* age simultaneously from all the high-mass stars (as in Section 5.2), but still found that the distance estimate was almost independent of age between 0 and 20 Myr.

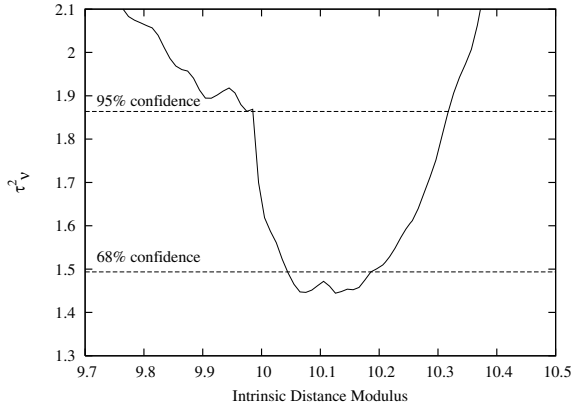

Figure 10. τ_ν^2 as a function of distance for the fit to the 10 Myr Geneva isochrone. The 68 and 95 per cent confidence levels are marked.

5.2 Low-mass isochrones

We can also estimate an age by fitting the positions of the spectroscopically confirmed low-mass members of NGC 2169 with isochrones from various PMS evolutionary models. The age derived in this way is *strongly* correlated with the assumed distance to the cluster. To make the correlation explicit, we again carried

Table 8. The parameters derived from PMS fits.

Model	Best fit		Age (Myr) for d_m	
	d_m (mag)	Age (Myr)	10.19	10.04
Geneva	10.13			
	(10.04–10.19 68 per cent)			
Baraffe	9.5	24	9.5	11.5
Siess	9.8	11	7.0	8.5
DAM97		>100	5.0	6.5

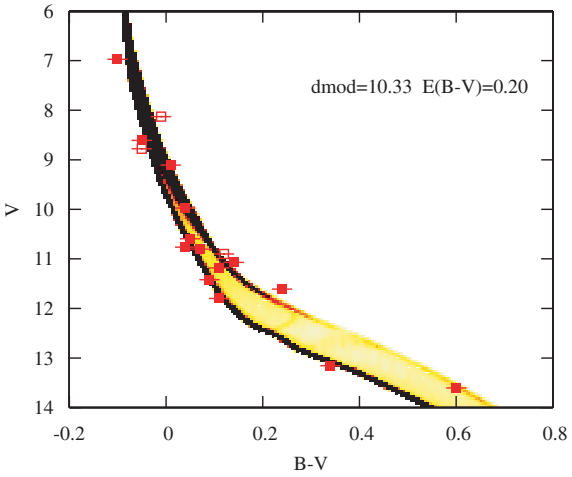

Figure 11. The best-fitting Geneva model with a 50 per cent binary frequency is represented with a grey-scale distribution. The data points from Sagar (1976) are shown with symbols as in Fig. 9. The brightest cluster member was not fitted (see text).

out τ^2 fits, this time allowing both age and distance modulus to be free parameters. We can then use this relationship along with the distance derived from the high-mass stars to find a best estimate for the age of NGC 2169. Significantly different ages (in the formal statistical sense) are found depending on which model we use. In what follows, we therefore consider each model in turn. For each model isochrone, effective temperature and bolometric luminosity were converted into I_C and $R_C - I_C$ using empirical relationships between colour and temperature and colour and bolometric correction. The colour–temperature relationship was established for each set of evolutionary models by demanding that an isochrone with an age of 120 Myr at a distance modulus of 5.6 and with an extinction $E(R_C - I_C) = 0.029$ matches the I_C versus $R_C - I_C$ locus of the Pleiades (see Jeffries, Thurston & Hambly 2001; Naylor et al. 2002; Jeffries & Oliveira 2005). For NGC 2169, we used an extinction of $E(R_C - I_C) = 0.14$, and for both clusters assumed $A_I/E(R_C - I_C) = 2.57$ (Dean, Warren & Cousins 1978; Taylor 1986). The bolometric correction was assumed to be a function of $R_C - I_C$, and obtained by fitting the colours of late-type dwarfs, as in Naylor et al. (2002). The main assumption in this method of 'tuning' the isochrones is that the relationships between temperature, bolometric correction and colour are the same at 120 Myr and at the ages of the isochrones that fit NGC 2169 [see Jeffries & Oliveira (2005) for a discussion of this point].

Since we are using PMS contraction to derive the age of the cluster, we wish to fit the lowest mass objects possible. The best data set to fit therefore is our own I_C versus $R_C - I_C$ photometry of members confirmed in Section 4.3. We fitted the 36 stars we identified as members, with the exception of target 45, which is marked as non-stellar in our catalogue due to the presence of a nearby bright star.

5.2.1 *The Baraffe isochrones*

Our baseline models were the isochrones of (Baraffe et al. 1998, 2002) (using the solar metallicity models with a convective mixing length set to 1.0 pressure scaleheights), with an assumed binary fraction of 50 per cent and uniform mass ratio distribution. Studies of the field binary population suggest these are reasonable assumptions for low-mass stars (e.g. Duquennoy & Mayor 1991; Fischer & Marcy 1992). Secondary stars which lie below the lowest mass available in the models were assumed to make a negligible contribution to the system light, which is equivalent to placing the binary on the single-star sequence. This limitation of the isochrones leads to the wedge of zero probability between the single- and binary-star sequences at low masses visible in Fig. 12.

A straightforward fit of this type leads to a $P_r(\tau^2)$ of 0.0025, after clipping out two data points. This is unacceptably low, and already includes the addition of a magnitude-independent uncertainty (0.01 mag in $R_C - I_C$) to all the data points to allow for the uncertainties in our profile correction and transformation to the standard system (see Section 3).

To account for this extra scatter and hence derive reliable uncertainties on the derived parameters, we increased the systematic uncertainties in the R and I_C measurements to 0.03 mag and obtain an acceptable $P_r(\tau^2) = 0.47$. This procedure can be considered analogous to increasing the uncertainties on each point in order to obtain $\chi^2_\nu \simeq 1$. The resulting parameters are given in Table 8 and the best-fit is shown in Fig. 12(a). The fit is a reasonable one, with the model explaining most of the spread in colour as due to binarity. Only at the faintest magnitudes is there a hint of any problem.

The most important result, however, is the τ^2 grid of Fig. 13(a), since we can combine it with the age constraint from the high-mass stars (Section 5.1). If we choose the lowest values of τ^2 at the 68 per cent confidence-limit distances, we obtain the age constraints given in Table 8.

5.2.2 *The Siess isochrones*

We also fitted the data to the Siess, Dufour & Forestini (2000) isochrones with metallicity $Z = 0.02$ and no convective overshoot. The resulting fit and τ^2 space are shown in Figs 12(b) and 13(b). Here, there is a problem with the faintest objects, because the models go no lower than 0.1 $M_\odot$. This means that the 'binary wedge' is very large, with the equal-mass binary sequence disappearing completely at quite bright magnitudes. We therefore removed the four objects fainter than $I_C = 18.3$. We obtain a best-fit at an age of 11 Myr and a distance modulus of 9.8. The $P_r(\tau^2)$ is 0.87, which although nominally better than the value obtained for the (Baraffe et al. 1998, 2002) isochrones, one should recall excludes a contribution from the faintest data points that contributed most to τ^2 for the Baraffe models.

5.2.3 *The DAM97 isochrones*

Finally, we carried out fits to the models of D'Antona & Mazzitelli (1997, hereafter the DAM97 isochrones). The formal fits to these isochrones imply NCG 2169 is very old (>100 Myr). This behaviour appears to be caused by the way the isochrones do not steepen at

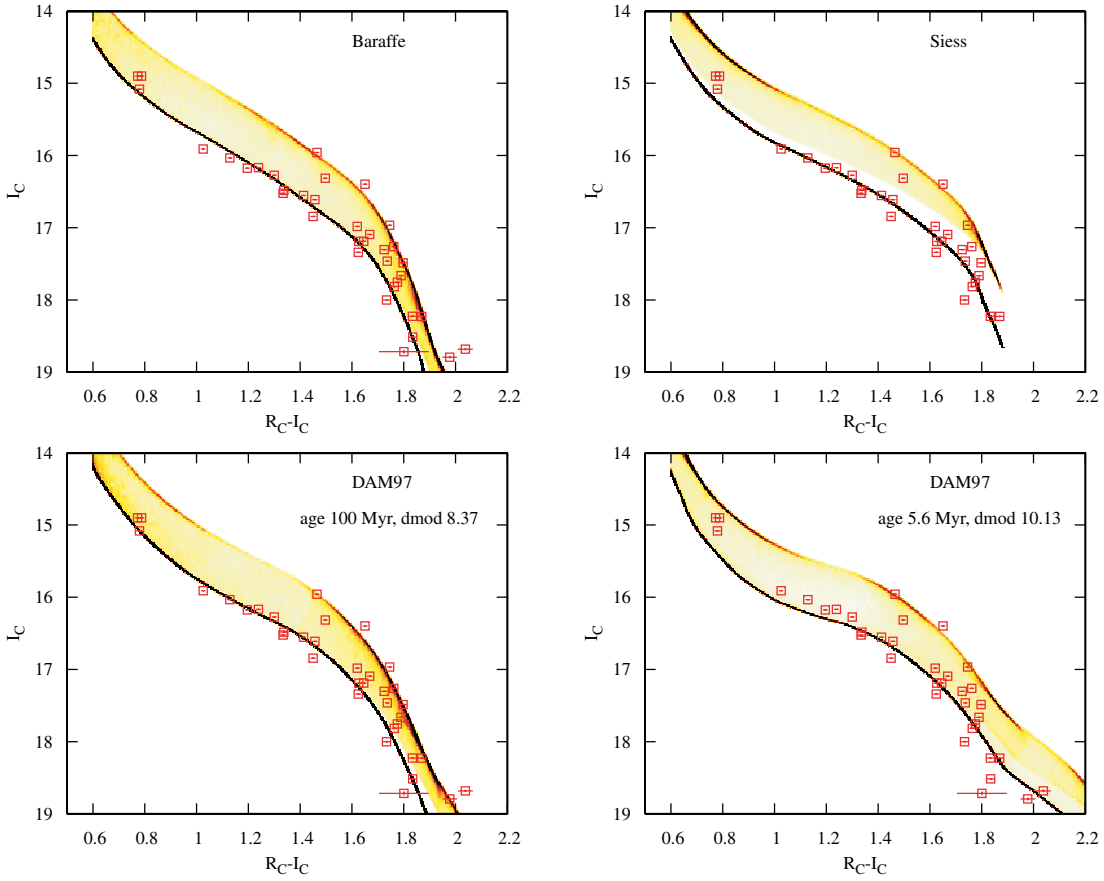

Figure 12. The best-fitting distributions using isochrones from several evolutionary models, a binary frequency of 50 per cent and a flat mass ratio distribution. The fitted data points are shown with error bars that *do not* include the 0.03 mag systematic error that is discussed in the text. The best-fitting age and distance are given in Table 8. (a) Isochrone from (Baraffe et al. 1998, 2002) using a mixing length of 1.0 pressure scaleheights; (b) isochrone from Siess et al. (2000) models with a metallicity of 0.02 and no convective overshoot; (c) isochrone from DAM97 and (d) isochrone from DAM97, but in this case the distance modulus is constrained to be 10.13 mag, the best-fitting value from the high-mass main sequence (see Section 5.1).

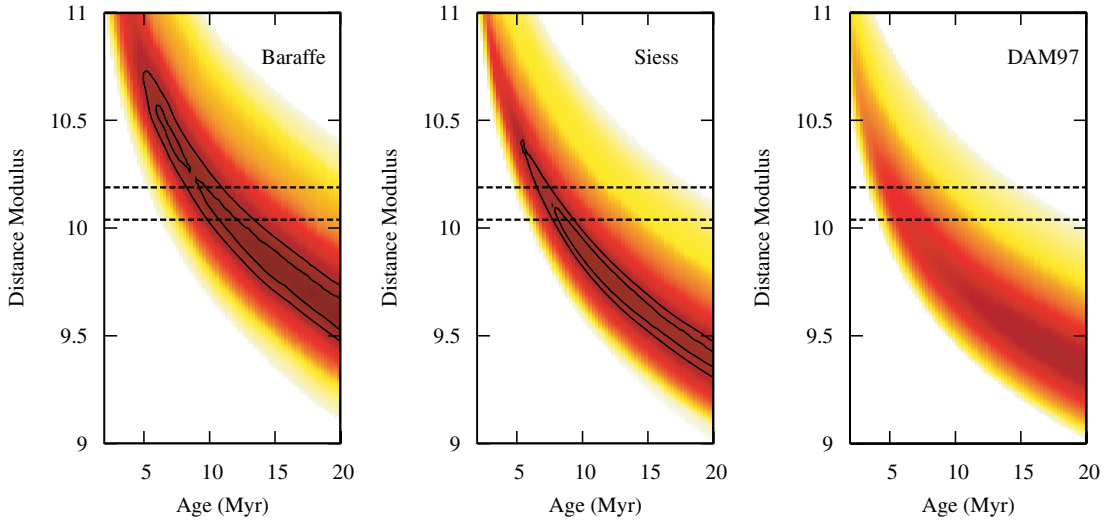

Figure 13. The τ^2 grid for the low-mass isochrone fits. The contour lines are the 68 and 95 per cent confidence limits. The horizontal lines are the 68 per cent confidence limits for the distance modulus derived from the main-sequence fitting to the higher mass stars (see Section 5.1). (a) (Baraffe et al. 1998, 2002) models with a mixing length of 1.0 pressure scaleheights. (b) The Siess et al. (2000) models with a metallicity of 0.02 and no convective overshoot. (c) The DAM97 models. In this latter case, the confidence limits lie at larger ages than displayed on the grid (see text).

$R_C - I_C > 1.7$ in contrast to the Baraffe and Siess isochrones. Older isochrones tend to be straighter, which clearly lead to better fits if the distance is unconstrained. The τ^2 grid for ages $\leqslant$20 Myr is shown in Fig. 13(c). Although the best-fitting distance is clearly far removed from the values given by the other models, the correct question to ask is whether the distances are co-incident at a given confidence level. As we have not found the lowest point in the τ^2 space, our normal method of finding the contour will over-estimate its size. Even then, we find that the youngest age enclosed by the 95 per cent confidence contour is 20 Myr (at a distance modulus of 9.4). The best-fitting model for a fixed distance modulus of 10.13 mag is shown in Fig. 12(d). As implied by Fig. 13(c), the fit is much worse. Hence, the DAM97 models are a poor description of the combined data set.

5.2.4 The age of NGC 2169

The numerical results of our fitting are summarized in Table 8. From this it can be seen that if the distance is constrained to be that implied by fits to the high-mass stars, then the DAM97 isochrones yield the youngest age, then Siess et al. (2000), and finally Baraffe et al. (1998, 2002). The ages derived using the 68 per cent confidence interval distance from the main-sequence fitting just fail to overlap, and hence the uncertainty in age is dominated by the choice of model, not by the data. Both the (Baraffe et al. 1998, 2002) and Siess et al. (2000) models satisfactorily fit the shape of the low-mass PMS at the distance implied by fits to the upper main sequence. Thus, our best estimate for the age of NGC 2169 is 9 ± 2 Myr, the upper limit defined by the Baraffe et al. models and the lower limit by the Siess et al. models.

That the DAM97 isochrones struggle to reproduce the low-mass PMS unless the distance modulus is allowed to become unreasonably low and the age unreasonably high does not necessarily rule them out. The discrepancies between data and model occur predominantly in the coolest stars where it is still possible that systematic uncertainties in the photometric calibration (in this study or in the Pleiades data which calibrate the colour–temperature relationship) could change the data–model comparison. However, if the coolest stars were to be made even redder to better match the isochrone shapes, then the derived age for the cluster would be even younger than 5 Myr.

5.3 The Li depletion age

That all of the firm cluster members have EW[Li] > 0.3 Å puts strong constraints on the age of NGC 2169. For clusters with ages $>$30 Myr, there is observational evidence that an 'Li depletion chasm' opens up, starting with stars at spectral type $\simeq$M2 and widening with age to encompass spectral types either side (see Jeffries 2006). The cool side of this chasm, the so-called Lithium depletion boundary, is sharp and almost model independent. It occurs when the cores of contracting, fully convective stars reach a temperature sufficient to burn Li. The warm side of the chasm exhibits a more gradual roll-off with temperature (see Fig. 14). Here, the depletion takes place at the boundary of a radiative core and a receding convective envelope. The amount of depletion is sensitively dependent on details of the convection treatment, interior opacities and chemical composition.

In principle, isochrones of Li depletion can be used as an alternative way to estimate the age of a cluster. The difficulties in doing so are converting the data in the observational plane (spectral type/colour and a spectrum or EW[Li]) into the quantities predicted by models (i.e. $T_{\rm eff}$ and a Li abundance) or vice versa. A further slight complication is that models predict Li depletion rather than Li abundance. The initial Li abundance must be assumed, although a value of A(Li) [$= 12 + \log {\rm N(Li)/N(H)}$] of 3.3 ± 0.1 appears to agree with observational constraints from meteorites and very young (presumably undepleted) stars (Soderblom et al. 1999).

We chose to perform a comparison of data and models in the observational plane of EW[Li] versus $R_C - I_C$ colour. Model temperatures were transformed using the same colour–$T_{\rm eff}$ relations required to make the same models match the Pleiades CMD (see Section 5.2). The predicted abundance was transformed into EW[Li] using $T_{\rm eff}$ and the relationship between abundance and EW[Li] derived from cool stellar atmospheres and synthetic spectra by Zapatero Osorio et al. (2002) and extended to warmer temperatures and lower abundances by Jeffries et al. (2003). This latter relationship was derived to interpret spectra with a spectral resolution of 1.68 Å and predicts 'pseudo-EWs' with respect to a local continuum. In this respect, it is ideal for interpreting our measured EWs.

The comparisons with four models are shown in Fig. 14. These are the isochrones arising from the Li depletion predicted by the (Baraffe et al. 1998, 2002) evolutionary tracks, using a mixing length of either 1.0 or 1.9 pressure scaleheights, respectively; the Siess et al. (2000) models with no convective overshoot and a mean metallicity of $Z = 0.02$ and the grey atmosphere models of DAM97 featuring the full spectrum turbulence treatment of convection.

Taking the observations at face value, the majority of targets appear to possess Li at undepleted levels, with one or two objects showing some evidence of depletion (amounting at most to about a factor of 10 in target 32). On the other hand, some of the coolest objects appear to show significantly enhanced Li with respect to the assumed initial abundance. One of these (target 28) has two mutually consistent measurements taken on different nights. Looking at the bulk of the objects, the Li measurements can only give upper limits to the cluster age. On the redwards side ($R_C - I_C > 1.5$), the lack of a clear cut lithium depletion boundary implies a cluster age of $<$15 Myr for all the models. For $R_C - I_C < 1.5$, there is some model dependence due to the increasing efficiency of convection as we move from the top left to bottom right of Fig. 14. The Baraffe models with mixing length of 1.0 scaleheights suggest an age $<$10 Myr for most stars with the possibility of a couple of objects as old as 15 Myr. Models with increased convective efficiency suggest progressively younger ages with the bulk of objects consistent with ages of $\leqslant$5 Myr and maximum ages of about 12, 10 and 8 Myr, respectively, for the Baraffe et al. model with larger mixing length, the Siess et al. model and the D'Antona & Mazzitelli model, respectively.

The ages inferred from the Li depletion are in reasonable agreement with those inferred from the low-mass isochronal fits using the same models. We do not find strong evidence for examples of anomalously rapid Li depletion amongst young stars that might imply a problem with the evolutionary models as suggested by Song et al. (2002) and White & Hillenbrand (2005).

6 CLUSTER STRUCTURE AND TOTAL MASS

Our spectroscopic membership determination can be used to define a selection region in the I_C versus $R_C - I_C$ CMD that preferentially includes cluster members and excludes contaminating objects. A larger sample of probable cluster members can then be chosen from our entire photometric survey and used to investigate the spatial distribution of low-mass stars in NGC 2169.

Fig. 15 shows a polygon that we have used to select photometric candidates with $15.5 < I_C < 19.0$. The appearance of Fig. 15 and

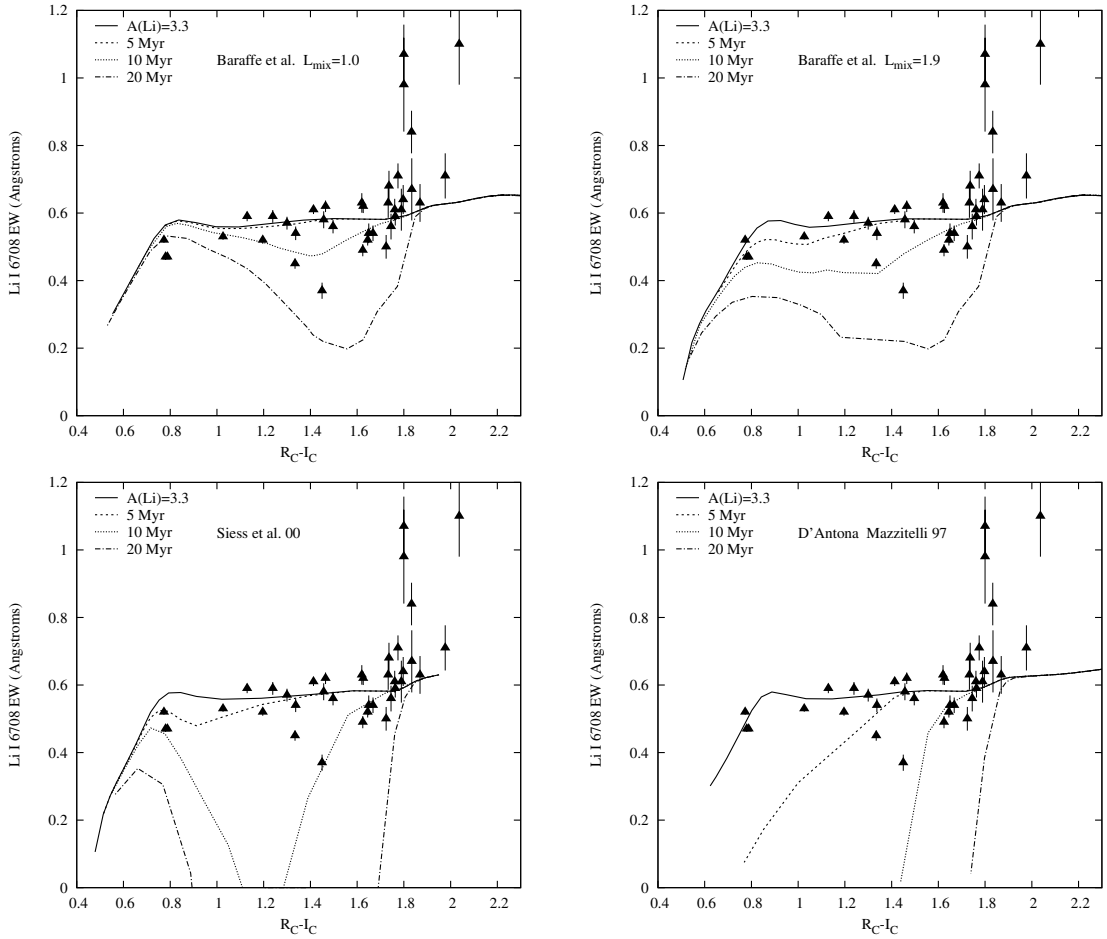

Figure 14. Isochrones (0, 5, 10 and 20 Myr) of EW[Li] versus $R_C - I_C$ derived from several different models and compared to our observations. An initial Li abundance of A(Li) = 3.3 is assumed and abundances are converted to EWs using the relationships defined in Zapatero Osorio et al. (2002) and Jeffries et al. (2003). (a) (Baraffe et al. 1998, 2002) using a mixing length of 1.0 pressure scaleheights. (b) (Baraffe et al. 1998, 2002) using a mixing length of 1.9 pressure scaleheights. (c) Siess et al. (2000) using a metallicity of $Z = 0.02$ and no overshooting. (d) DAM97 using a grey atmosphere and the full spectrum turbulence treatment of convection.

also Fig. 2 suggests that few cluster members could lie redwards or bluewards of the polygon boundaries. We have applied this photometric selection criterion to our entire catalogue (Table 3), and the resulting cluster candidates are plotted in Fig. 1 to show their spatial distribution. There are 64 photometric candidates in the $\sim$70 arcmin^2 defined by the overlapping GMOS fields, 38 of which were among our spectroscopic targets. Of these, 33 are Li-rich cluster members, two are non-members without Li and three have uncertain membership because of the lack of an EW[Li] measurement. From this, we deduce that the spatial density of contaminating non-members in our selection box is $\simeq$0.05 stars arcmin^{-2}. Incompleteness due to any lack of sensitivity in the photometric survey can be neglected at these magnitudes, although our choice of photometric selection boundaries, which deliberately excludes non-members, may have biased the non-member density downwards.

Fig. 1 shows a spatial concentration of photometric cluster candidates. By fitting a Gaussian plus a constant term to the spatial distribution along the RA and Dec. axes, we find the centre of this concentration to be at RA = $06^h08^m26(\pm4)^s$, Dec. = $+13^d58^m23(\pm18)^s$. The radial distribution of the candidates about this centre is shown in Fig. 16. We have corrected for incompleteness in coverage (e.g. due to proximity of bright stars), the azimuthal asymmetry in the survey extent and gaps in the CCD mosaic by normalizing with a similar distribution for stars with $15.5 < I_C < 19.0$ which are bluewards of the candidate cluster members. The radial distribution has been modelled with a King profile (see King 1962) plus a constant background density. The tidal radius of a cluster in the solar vicinity is given by $r_t = 1.46\,M_c^{1/3}$ (see Pinfield, Hodgkin & Jameson 1998). We assume that the mass of the cluster, M_c = 300 $M_\odot$ (see below), yielding r_t = 9.8 pc, equivalent to 32.2 arcmin for a distance modulus of 10.1 (see Section 5). The best-fitting core radius, normalization and background density are quite insensitive to r_t and hence very insensitive to the assumed cluster mass. The best-fitting King profile (shown in Fig. 16) has a core radius of (2.8 $\pm$ 1.0) arcmin (equivalent to 0.85 pc at a distance modulus of 10.1), a normalization of (1.7 $\pm$ 0.6) stars arcmin^{-2}, a constant background of (0.23 $\pm$ 0.03) stars arcmin^{-2} and a total of 87 cluster stars integrated out to the tidal radius. This background density is far in excess of that deduced from the spectroscopy above.

If we believe that the cluster spatial distribution *is* well represented by this King profile, then the majority (approximately 220) of the 302 photometric candidates plotted in Fig. 1 must be field stars and we would have been fortunate to observe only two non-members among 35 GMOS targets with Li measurements, rather than the

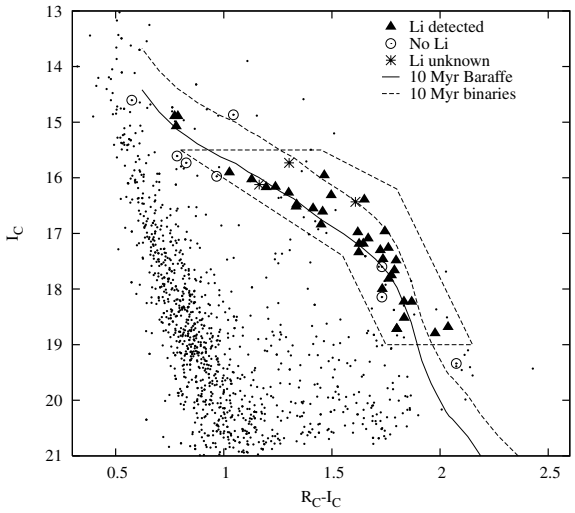

Figure 15. A CMD for the area covered by the three GMOS fields (see Fig. 1). Stars with Li (members), those without Li (non-members) and those with unknown Li (questionable membership) according to Section 4.3 are indicated. The dashed polygon indicates a region we have chosen for photometric selection of cluster members with $15.5 < I_C < 19.0$. Also shown are an isochrone and binary sequence from Baraffe et al. (2002 – with mixing length set at 1.0 pressure scaleheight) corresponding to an age of 10 Myr and intrinsic distance modulus of 10.13 (see Section 5).

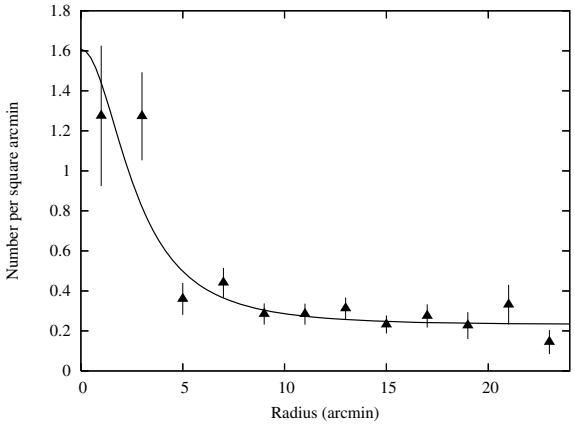

Figure 16. Radial surface density profile for photometric cluster candidates with $15.5 < I_C < 19.0$. The best-fitting King profile is shown.

nine that would be predicted on the basis of the fitted background described above.

We can also check whether the MF of the cluster is close to what has been seen in other clusters and the field. The limits of $15.5 < I_C < 19.0$ correspond closely to mass limits of $1.0 > M/\mathrm{M}_\odot > 0.15$ using a 10 Myr isochrone from (Baraffe et al. 1998, 2002) and a distance modulus of 10.13 (see Section 5). Choice of evolutionary model and variations of age and distance within the allowed uncertainties discussed in Section 5 can change these limits by ∼10 per cent, but do not change the basic argument set out below.

Using the universal piecewise power-law MF advocated by Kroupa (2001), which matches data from the field and many open clusters, then 87 stars with $0.15 < M/\mathrm{M}_\odot < 1.0$ should be found in a cluster with 3.9 stars with $2.5 < M/\mathrm{M}_\odot < 15.0$, corresponding to $1.2 > M_V > -4.1$ according to the 10 Myr Geneva isochrone used in Section 5.1. Fig. 9 shows there are at least 12–15 such stars in NGC 2169. Therefore, either (i) most of these high-mass stars do not belong to NGC 2169; (ii) the cluster IMF is deficient by a factor of ≃3 in low-mass stars or (iii) the good match of the King profile to the spatial distribution is coincidental and most of the 'background' in Fig. 16 is a population of low-mass cluster members extending out to the tidal radius and which is *much* more widely dispersed than the high-mass population. A King profile with the background fixed at the 0.05 stars arcmin^{-2} implied by spectroscopy in the GMOS fields is a poor fit (rejected at >99.99 per cent confidence) to the data.

In our view, both (i) and (ii) are unlikely, but confirming that the widely dispersed low-mass cluster candidates are genuine members would require further spectroscopy. For scenario (ii), the total mass of the cluster (for $0.15 < M/\mathrm{M}_\odot < 15.0$) is ≃150 $\mathrm{M}_\odot$, whereas for scenario (iii) the total mass is about 300 $\mathrm{M}_\odot$ if the Kroupa (2001) MF is assumed.

7 DISCUSSION

7.1 The age spread in NGC 2169

The possibility of age *spreads* in young clusters and star-forming regions has been vigorously debated. Whether molecular clouds can sustain star formation for long periods of time (∼10 Myr) or whether star formation is a rapid process that is essentially completed in a free-fall time (∼1 Myr) is related to whether magnetic fields or supersonic turbulence regulates the gravitational collapse of the clouds (e.g. Mac Low & Klessen 2004; Mouschovias, Tassis & Kunz 2006).

The age distribution of stars can be deduced from their position in HR diagrams. Based on several nearby star-forming regions including Taurus and the Orion Nebula cluster (ONC), the claim has been made that star formation accelerates over the course of ∼10 Myr in a typical molecular cloud (Palla & Stahler 2000, 2002). These claims are disputed by (Hartmann 2001, 2003) who explain apparent age spreads and accelerating formation rates in the HR diagram as due to binarity, variability, dispersion in extinction and accretion properties and contamination by foreground non-members [see also the discussion of variability in Burningham et al. (2005)]. Palla et al. (2005) have recently bolstered the idea of a significant age spread with the observation of several objects in the ONC that may have depleted their photospheric Li by factors of 3–10. They argue that such depletion could not occur unless these stars were at least 10 Myr old and that such ages are roughly in agreement with their positions in the HR diagram. The possible problem we see here is that Palla et al. (2005) needed to 'unveil' their spectra prior to determining the Li abundances, implying that the objects were heavily accreting. It is not clear that a plane-parallel, LTE model will satisfactorily yield Li abundances in these circumstances. The Li I 6708 Å resonance doublet forms close to the top of the atmosphere and is vulnerable to non-local thermodynamic equilibrium (NLTE) effects such as overionization by a non-photospheric ultraviolet (UV) continuum that could weaken EW[Li] (e.g. Houdebeine & Doyle 1995)

At an age of 9 ± 2 Myr, NGC 2169 is a fascinating cluster with which to test some of these ideas. First, accretion appears to have ceased (see Section 4.2.3), but the cluster is young enough that small changes in age still result in significant changes in luminosity for low-mass stars. Hence, the scatter of stars in the HR diagram will contain information on any age spread if it can be separated from scatter caused by binarity, intrinsic variability and differential reddening. Second, Li depletion only begins in low-mass stars after about 5–10 Myr, so for a given age spread any spread in Li depletion

should become much more pronounced in NGC 2169 than in a younger cluster like the ONC.

In Section 5.2, we found that a magnitude-independent uncertainty of 0.03 mag needed to be added to the uncertainty in each photometric band in order for the (Baraffe et al. 1998, 2002) models to provide a reasonable fit to the low-mass PMS. There could be several contributions to the requirement for this additional uncertainty: (i) that the isochrone shapes do not represent the data very well; (ii) variability due to chromospheric activity and starpots; (iii) differential reddening; (iv) incorrect assumptions about the binary frequency or mass ratio distribution; (v) an age spread. Of these, (i) appears not to be an issue (see Fig. 12a), (iii) is probably limited to less than 0.014 mag scatter in $E(R_C - I_C)$ (Delgado et al. 1992) and (iv) has little effect when changed within reasonable limits. Instead, it seems that there is additional scatter about the best-fitting isochrone (especially towards the low-mass end) that could be caused by a combination of (ii) and (v), but also includes a contribution of 0.01 mag from systematic photometric uncertainties (see Section 3).

The additional scatter corresponds to *at most* ± 0.04 mag (1 sigma) in $R_C - I_C$. Over the mass range of our cluster members, isochrones over a small age range are nearly parallel and a 0.04 mag dispersion is equivalent to only ± 1.2 Myr when translated into a shift in age (independent of which models are chosen). As young stars are known to be variable, this must represent an upper limit to how much of the scatter in the CMD can actually be attributed to an age spread. Of course, one could relax some of the (we believe very reasonable) assumptions about the binary frequency and mass ratio distributions to increase this, but even without any binary systems, the total age spread would be less than 10 Myr. A further concern might be that our spectroscopic target selection has prevented the inclusion of older cluster members that lie below the targeted cluster members in the CMD. Fig. 15 shows that there is a significant gap between the cluster members and what are presumably objects unassociated with the cluster that lie some way below the cluster main sequence. If they were cluster members, they would need to be at least 30 Myr old, which seems an unrealistically large spread. Our conclusion is that we do not require age spreads beyond a Gaussian FWHM of 2.5 Myr to explain the photometric data in NGC 2169.

Supporting evidence for a small age spread comes from the lack of any large dispersion in the Li abundances. This evidence has the additional merit of being independent of assumptions about binary frequencies, differential extinction or variability. Although we have already expressed our reservations about using the Li I 6708 Å line to derive Li abundances, it is likely that interpretation and modelling problems could only serve to increase the observed dispersion. Indeed, Fig. 14 shows several cooler objects that appear to have enhanced Li abundances. The Li observations imply age spreads of less than 10 Myr for all the models and as the dispersion must include a significant component from uncertainties in the Li abundances then this must be very much an upper limit. There is just one object (target 32) that may be significantly Li-depleted and have an age that is 5–10 Myr older than all the other cluster members. However, an age >5 Myr older than the majority of cluster members for target 32 is not supported by its position in the CMD. Hence, we do not find evidence of Li depletion similar to that found in the ONC by Palla et al. (2005) that might support an age spread as large as 10 Myr.

7.2 Accretion disc lifetimes

The time-scale for the disappearance of accretion signatures in young low-mass stars is a valuable probe of infalling gas and the evolution of the inner discs in protoplanetary systems. Broad and strong Hα emission is the most readily available signature of a strong accretion process. Finding the fraction of stars which exhibit such a signature as a function of age has been the goal of several recent investigations (e.g. Mohanty, Jayawardhana & Basri 2005; Sicilia-Aguilar et al. 2005). NGC 2169 occupies an important position, because at a similar age, studies of accretion disc evolution have largely been confined to sparsely populated nearby moving groups like η Chamaeleontis and TW Hya (e.g. Jayawardhana et al. 2006).

All of our NGC 2169 targets have EW[Hα] below the empirical accretion thresholds proposed by White & Basri (2003) and Barrado y Navascués & Martín (2003). None of the targets for which we have the necessary data shows a *K*-band near-infrared excess indicative of warm circumstellar material. However, a low-accretion rate or unfortunate geometric arrangement of the accretion disc and/or flow could result in a small EW[Hα] or broadened Hα emission with an EW below these thresholds (e.g. Muzerolle et al. 2000). Only one object in our sample (target 13) shows a broadened Hα emission line that might indicate a low level of accretion. Comparing Hα EWs with mass accretion rates derived from *U*-band excesses (Sicilia-Aguilar et al. 2005) suggests that the White & Basri (2003) Hα EW criterion corresponds to mass accretion rates of $\simeq 10^{-9}$ M$_\odot$ yr^{-1} for late-K and early-M stars, although variations in system geometry, viewing angle and the stellar mass will blur this boundary.

If we strictly adopt the White & Basri EW[Hα] accretion criterion, then the 95 per cent upper limits to the fraction of stars exhibiting accretion or *K*-band near-infrared excess in NGC 2169 are 8 (0/36) and 10 (0/30) per cent, respectively. The fraction of accretors in NGC 2169 is compared to other clusters in Fig. 17. We have chosen clusters from Mohanty et al. (2005), Sicilia-Aguilar et al. (2005), Dahm (2005) and Jayawardhana et al. (2006) where the fraction of accretors has been (re)determined based on the White & Basri (2003) EW[Hα] criteria, where all the cluster ages have been determined using the Baraffe et al. (1998) or Siess et al. (2000) models and where the mass range of the stars considered is similar to those in

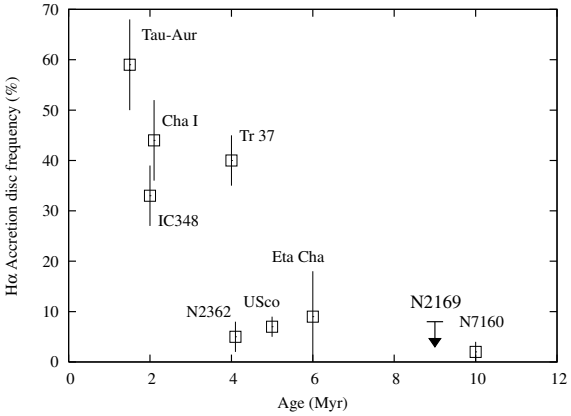

Figure 17. The fraction of low-mass stars in NGC 2169 that have accretion signatures [according to the White & Basri (2003) EW[Hα] criteria] compared with other clusters and associations as a function of age [derived from the Baraffe et al. (1998, 2002) or Siess et al. (2000) models]. The data come from Mohanty et al. (2005) for Taurus–Auriga, IC 348, Chamaeleon I and Upper Sco, from Dahm (2005) for NGC 2362, from Sicilia-Aguilar et al. (2005) for Tr 37 and NGC 7160, and from Jayawardhana et al. (2006) for the η Cha group. The relative precisions for the cluster ages are typically $\pm$1–2 Myr.

NGC 2169. The data for NGC 2169 strongly reinforce the view that significant gas accretion ($\gtrsim 10^{-9}\,M_\odot\,yr^{-1}$) has ceased at ages of 10 Myr in the vast majority of low-mass stars.

8 SUMMARY

The main findings of this paper can be summarized as follows.

(i) We have uncovered the low-mass population of NGC 2169, spectroscopically confirming 36 objects with $0.15 < M/M_\odot < 1.3$ as cluster members on the basis of their Li abundances, Hα emission and radial velocities. We provide a catalogue of these spectroscopic members and a full catalogue of $R_C I_C$ photometry covering 880 arcmin^2 around the cluster which contains several hundred other photometric candidates (see below).

(ii) The high-mass population of the cluster has been used to estimate an intrinsic distance modulus of $10.13^{+0.06}_{-0.09}$ mag. At this distance, isochrone fitting with several low-mass evolutionary models yields ages from 5 to 11 Myr. The age from the (Baraffe et al. 1998, 2002) and Siess et al. (2000) models, which provide the best description of the low-mass data, is 9 ± 2 Myr. Age constraints from the main-sequence turn-off and from estimates of Li depletion in the low-mass stars are consistent with this age.

(iii) Using reasonable assumptions for the binary frequency and mass ratio distribution, the low-mass isochronal fits do not require any age spread in the cluster population beyond a Gaussian FWHM of 2.5 Myr. The observed levels of Li depletion are also consistent with a small age spread (<10 Myr) and only one M-type cluster member shows any evidence of significant Li depletion that might indicate it is >5 Myr older than the rest of the cluster. Hence, the observations do not support scenarios where significant star formation in a cluster proceeds over extended periods of time ($\gtrsim$5 Myr).

(iv) On the basis of the strength and width of their Hα emission lines and the lack of any *K*-band near-infrared excesses, we find no strong evidence of accretion activity or warm circumstellar material in the confirmed cluster members. Comparison with younger clusters reinforces the idea that significant levels of gas accretion cease on time-scales <10 Myr for the vast majority of low-mass stars.

(v) Informed by the spectroscopically confirmed cluster members, we have photometrically selected several hundred other low-mass cluster candidates. A consideration of the number and spatial distribution of these candidates suggests either that the cluster has a 'top–heavy' MF or that the cluster's low-mass stars are much more widely distributed than the high-mass stars – out to radii of 20 arcmin. The total cluster mass for stars of $0.15 < M/M_\odot < 15$ is 150–300 $M_\odot$.

Although much further away, the low-mass population of NGC 2169 is larger than those in the kinematically defined groups in the solar vicinity (e.g. η Cha, TW Hya) which have so far provided the focus for investigations of the early evolution of stars and planetary systems at a similar age. Nearby moving groups will continue to provide the best targets for programmes such as direct imaging, where spatial resolution is crucial, but clusters like NGC 2169 offer much more potential for precise statistical investigations of low-mass stellar properties such as spectral energy distributions, rotation rates and X-ray activity. The greater distance will frequently be offset (as in this paper) by the multiplexing capability of multi-object or wide-field instruments that can observe many low-mass objects simultaneously.

ACKNOWLEDGMENTS

Based on observations obtained at the *Gemini* Observatory (program GN-2005B-Q-30), which is operated by the Association of Universities for Research in Astronomy, Inc., under a cooperative agreement with the NSF on behalf of the *Gemini* partnership: the National Science Foundation (United States), the Particle Physics and Astronomy Research Council (United Kingdom), the National Research Council (Canada), CONICYT (Chile), the Australian Research Council (Australia), CNPq (Brazil) and CONICET (Argentina). Also based on observations made with the INT which is operated on the island of La Palma by the Isaac Newton Group in the Spanish Observatorio del Roque de los Muchachos of the Instituto de Astrofisica de Canarias.

This publication makes use of data products from the 2MASS, which is a joint project of the University of Massachusetts and the Infrared Processing and Analysis Center/California Institute of Technology, funded by the National Aeronautics and Space Administration and the National Science Foundation. NJM acknowledges the receipt of a studentship funded by the UK Particle Physics and Astronomy Research Council.

REFERENCES

Abt H. A., 1977, PASP, 89, 646
Bailer-Jones C. A. L., 2004, A&A, 419, 385
Baraffe I., Chabrier G., Allard F., Hauschildt P. H., 1998, A&A, 337, 403
Baraffe I., Chabrier G., Allard F., Hauschildt P. H., 2002, A&A, 382, 563
Barrado y Navascués D., Martín E. L., 2003, AJ, 126, 2997
Barrado y Navascués D., Stauffer J. R., Jayawardhana R., 2004, ApJ, 614, 386
Bessell M. S., Brett J. M., 1988, PASP, 100, 1134
Burningham B., Naylor T., Jeffries R. D., Devey C. R., 2003, MNRAS, 346, 1143
Burningham B., Naylor T., Littlefair S. P., Jeffries R. D., 2005, MNRAS, 363, 1389
Chiosi C., Bertelli G., Bressan A., 1992, ARA&A, 30, 235
Cuffey J., McCuskey S. W., 1956, ApJ, 123, 59
Dahm S. E., 2005, AJ, 130, 1805
D'Antona F., Mazzitelli I., 1997, Mem. Soc. Astr. It., 68, 807 (DAM97)
Dean J. F., Warren P. R., Cousins A. W. J., 1978, MNRAS, 183, 569
Delgado A. J., Alfaro E. J., Garcia-Pelayo J. M., Garrido R., 1992, AJ, 103, 891
Duquennoy A., Mayor M., 1991, A&A, 248, 485
Fischer D. A., Marcy G. W., 1992, ApJ, 396, 178
Harris G. L. H., 1976, ApJS, 30, 451
Hartmann L., 2001, AJ, 121, 1030
Hartmann L., 2003, ApJ, 585, 398
Hoag A. A., Johnson H. L., Iriarte B., Mitchell R. I., Hallam K. L., Sharpless S., 1961, Publ. U.S. Naval Obs., 17, 343
Houdebeine E., Doyle J. G., 1995, A&A, 302, 861
Jayawardhana R., Coffey J., Scholz A., Brandeker A., van Kerkwijk M. H., 2006, ApJ, 648, 1206
Jeffries R. D., 2006, in Randich S., Pasquini L., eds, Chemical Abundances and Mixing in Stars in the Milky Way and its Satellites. Springer, New York, p. 163
Jeffries R. D., Oliveira J. M., 2005, MNRAS, 358, 13
Jeffries R. D., Thurston M. R., Hambly N. C., 2001, A&A, 375, 863
Jeffries R. D., Oliveira J. M., Barrado y Navascués D., Stauffer J. R., 2003, MNRAS, 343, 1271
Jenniskens P., Desert F.-X., 1994, A&AS, 106, 39
Jerzykiewicz M., Kopacki G., Molenda-Zakowicz J., Kolaczkowski Z., 2003, Acta Astron., 53, 151
Jones B. F., Shetrone M., Fischer D., Soderblom D. R., 1996, AJ, 112, 186
King I. R., 1962, AJ, 67, 471

Kroupa P., 2001, MNRAS, 322, 231
Landolt A., 1992, AJ, 104, 340
Leggett S. K., 1992, ApJS, 82, 351
Lejeune T., Schaerer D., 2001, A&A, 366, 538
Littlefair S. P., Naylor T., Harries T. J., Retter A., O'Toole S., 2004, MNRAS, 347, 937
Liu T., Janes K. A., Bania T. M., 1989, AJ, 98, 626
Lyra W., Moitinho A., van der Bliek N. S., Alves J., 2006, A&A, 453, 101
Mac Low M.-M., Klessen R. S., 2004, Rev. Modern Phys., 76, 125
Meynet G., Maeder A., 1997, A&A, 321, 465
Meynet G., Maeder A., 2000, A&A, 361, 101
Mohanty S., Jayawardhana R., Basri G., 2005, ApJ, 626, 498
Mouschovias T. C., Tassis K., Kunz M. W., 2006, ApJ, 646, 1043
Muzerolle J., Briceño C., Calvet N., Hartmann L., Hillenbrand L., Gullbring E., 2000, ApJ, 545, L141
Muzerolle J., Calvet N., Hartmann L., 1998, ApJ, 492, 743
Naylor T., 1998, MNRAS, 296, 339
Naylor T., Jeffries R. D., 2006, MNRAS, 373, 1251
Naylor T., Totten E. J., Jeffries R. D., Pozzo M., Devey C. R., Thompson S. A., 2002, MNRAS, 335, 291
Oliveira J. M., Jeffries R. D., Devey C. R., Barrado y Navascués D., Naylor T., Stauffer J. R., Totten E. J., 2003, MNRAS, 342, 651
Palla F., Stahler S. W., 2000, ApJ, 540, 255
Palla F., Stahler S. W., 2002, ApJ, 581, 1194
Palla F., Randich S., Flaccomio E., Pallavicini R., 2005, ApJ, 626, L49
Peña J. H., Peniche R., 1994, Rev. Mex. Astron. Astrofis., 28, 139
Perry C. L., Lee P. D., Barnes J. V., 1978, PASP, 90, 73
Pinfield D. J., Hodgkin S. T., Jameson R. F., 1998, MNRAS, 299, 955
Piskunov A. E., Belikov A. N., Kharchenko N. V., Sagar R., Subramaniam A., 2004, MNRAS, 349, 1449
Randich S., Pallavicini R., Meola G., Stauffer J. R., Balachandran S., 2001, A&A, 372, 862
Rastorguev A. S., Glushkova E. V., Dambis A. K., Zabolotskikh M. V., 1999, Astron. Lett., 25, 595
Rieke G. H., Lebofsky M. J., 1985, ApJ, 288, 618
Ruprecht J., 1966, Bull. Astron. Inst. Czechoslovakia, 17, 33
Sagar R., 1976, Ap&SS, 40, 447
Schaller G., Schaerer D., Meynet G., Maeder A., 1992, A&AS, 96, 269
Schlesinger B. M., 1972, AJ, 77, 584
Sicilia-Aguilar A., Hartmann L. W., Hernández J., Briceño C., Calvet N., 2005, AJ, 130, 188
Siess L., Dufour E., Forestini M., 2000, A&A, 358, 593
Skrutskie M. F. et al., 2006, AJ, 131, 1163
Soderblom D. R., Jones B. F., Balachandran S., Stauffer J. R., Duncan D. K., Fedele S. B., Hudon J. D., 1993, AJ, 106, 1059
Soderblom D. R., King J. R., Siess L., Jones B. F., Fischer D., 1999, AJ, 118, 1301
Song I., Bessell M. S., Zuckerman B., 2002, ApJ, 581, L43
Stauffer J. R. et al., 1999, ApJ, 527, 219
Stauffer J. R., Schultz G., Kirkpatrick J. D., 1998, ApJ, 499, L199
Stetson P. B., 2000, PASP, 112, 925
Taylor B. J., 1986, ApJS, 60, 577
White R. J., Basri G., 2003, ApJ, 582, 1109
White R. J., Hillenbrand L. A., 2005, ApJ, 621, L65
Zapatero Osorio M. R., Béjar V. J. S., Pavlenko Y., Rebolo R., Allende Prieto C., Martín E. L., García López R. J., 2002, A&A, 384, 937

SUPPLEMENTARY MATERIAL

The following supplementary material is available for this article.

Table 3. The R_C versus $R_C - I_C$ photometric catalogue.

This material is available as part of the online article from http://www.blackwell-synergy.com/doi/abs/10.1111/j.1365-2966.2006.11327.x. (This link will take you to the article abstract.)

Please note: Blackwell Publishing are not responsible for the content or functionality of any supplementary materials supplied by the authors. Any queries (other than missing material) should be directed to the corresponding author for the article.

This paper has been typeset from a TEX/LATEX file prepared by the author.